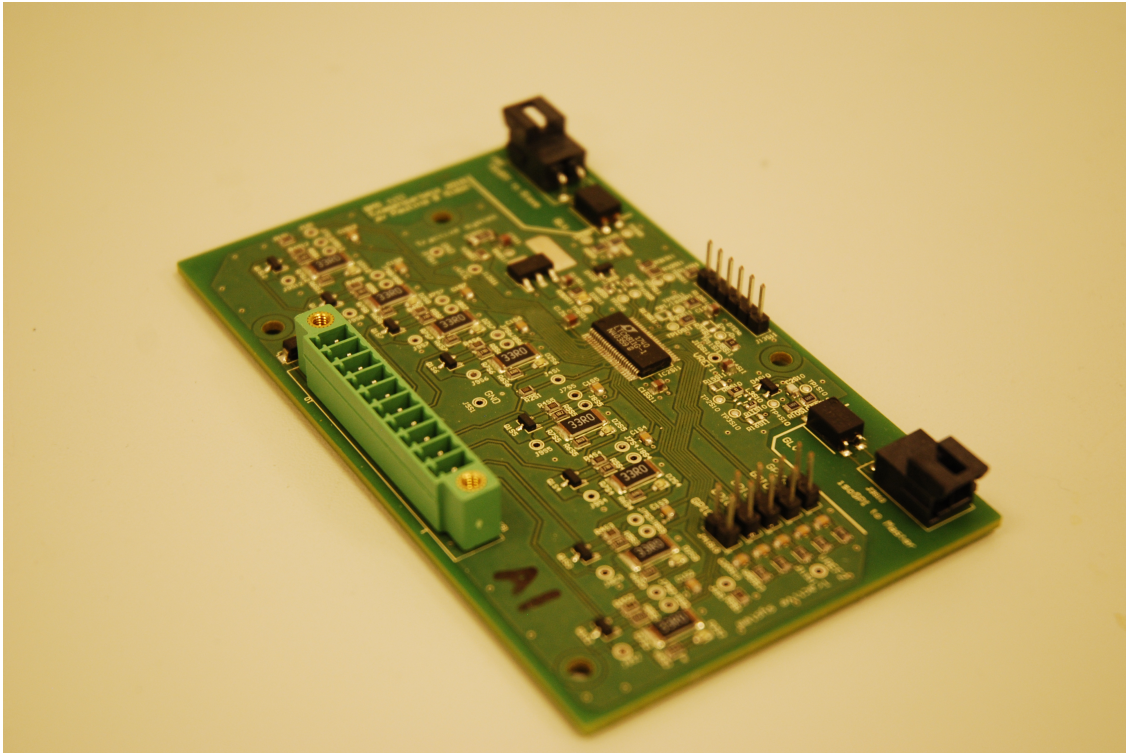




CHALMERS
UNIVERSITY OF TECHNOLOGY



Battery Management System

State of Charge Estimations

Master's thesis in Electric Power Engineering

Paulina Eriksson, Simon Nilsson

MASTER THESIS 2018-06

Battery Management System State of Charge Estimations

Paulina Eriksson
Simon Nilsson



Department of Electrical Engineering
Division of Electrical Engineering
CHALMERS UNIVERSITY OF TECHNOLOGY
Gothenburg, Sweden 2018

Battery Management System
State of Charge Estimations
PAULINA ERIKSSON
SIMON NILSSON

© PAULINA ERIKSSON, SIMON NILSSON, 2018.

Supervisor: Lucia El-Achkar, QRTECH AB
Supervisor: Matilda Hildesson, QRTECH AB
Examiner: Torbjörn Thiringer, Department of Electric Power Engineering

Master Thesis 2018:06
Department of Electrical Engineering
Division of Electric Power Engineering
Chalmers University of Technology
SE-412 96 Gothenburg
Telephone +46 31 772 1000

Cover: Picture of the hardware performing voltage and temperature measurements in the battery management system.

Battery Management System
State of Charge Estimations
PAULINA ERIKSSON
SIMON NILSSON
Department of Electrical Engineering
Chalmers University of Technology

Abstract

Restrictions on tailpipe emissions from vehicles have driven the vehicle industry towards electrified vehicles with lithium cells. The cells have an arrow operating window, which brings the need for a Battery Management Systems (BMS). The purpose with this thesis is to develop a semi-distributed scalable BMS for an electric go-kart with a $LiFePO_4$ battery. The individual cell voltage and temperature measurements are performed by the Multicell Battery Monitor LTC6811-1 on the custom designed PCB:s. The control system of the BMS is developed in MatlabSimulink and code generated to an Electronic Control Unit (ECU). The control system estimates State of Charge (SOC) using a combination of the Coulomb Counting (CC) method and the Open Circuit Voltage (OCV) method.

An improper time period setting in the ECU and the measuring accuracy of the voltage and the current, greatly affected the SOC estimations, as a result the estimations had low accuracy. However it has been shown that the overall design of the BMS is functioning properly with the data it receives. For better estimations, more accurate current measurement and voltage data for the OCV method are needed.

Keywords: BMS, EV, SOC, OCV and CC.

Acknowledgements

The knowledge that can be found when wandering around the corridors at QRTECH AB has been invaluable for this thesis. The guidance, encouragement and joy received from our supervisors Lucia El-Achkar and Matilda Hildesson is what made the project possible. A special thanks to Joakim Hesselgren who has been able to guide two hardware engineers throughout the slippery slope of C coding. Carl Petersson and Filip Pettersson we would like to thank for the help with the hardware design and test procedures. To Zeyang Geng for your invaluable guidance regarding lithium ion batteries. We would also like to thank our examiner Torbjörn Thiringer, who has given us guidance throughout the thesis.

Paulina Eriksson, Simon Nilsson, Gothenburg, June 2018

Contents

1	Introduction	1
1.1	Problem background	1
1.2	Previous work	2
1.3	Purpose	2
2	Battery modelling and BMS theory	3
2.1	Battery modelling	3
2.2	BMS	5
2.3	SOC estimation methods	5
2.3.1	OCV method	5
2.3.2	Coulomb counting method	6
2.4	Battery balancing	6
3	Simulation set-up	9
3.1	Battery cell model	9
3.2	BMS model	9
3.2.1	SOC estimators	9
3.2.2	Battery balancing	10
3.2.3	Fault detection	10
4	BMS Design	13
4.1	Go-kart specification	13
4.2	Hardware	14
4.2.1	Voltage measurement	15
4.2.2	Temperature measurement	16
4.2.3	Current measurement	17
4.2.4	Battery Balancing	17
4.2.5	Communication	19
4.3	Software	19
5	Measurement set-up	23
5.1	Battery parameter extraction	23
5.2	BMS verification	24
6	Analysis of the BMS	25
6.1	Cell parameters and characteristics	25
6.1.1	OCV	25

6.1.2	Energy content	27
6.1.3	EIS	29
6.2	SOC estimation verification	31
7	Conclusion	37
7.1	Results from present work	37
7.2	Future work	38
	Bibliography	41
	Appendices	43
A	Appendix: Figures of the simulation set-up	43
B	Appendix: Figures with outliers	51
C	Appendix: Datasheet of Headway 40152S cells	53
D	Appendix: Datasheet of A123: HTPFR18650-1100mAh-3.2V cells	57

1

Introduction

1.1 Problem background

Restrictions on tailpipe emissions from vehicles have driven the vehicle industry towards Electrified Vehicles (EV:s) and at the same time the demand of mobile electric devices like robots, laptops and cellphones have increased rapidly during the last decade. This has lead to a very high demand of electric energy storage solutions [1]. Today Lithium Ion Batteries (LIB) are totally dominating in this sector because of their high power density and cost effectiveness compared to other solutions [1].

A LIB has a narrow operating range, in regards to voltage, current and temperature. This makes it essential to monitor/estimate and control these parameters directly or indirectly with a BMS to keep the LIB in a safe operation region [2].

The BMS measures and estimates a number of parameters where the more important can be terminal voltage, drawn current, State Of Charge (SOC), State Of Health (SOH), temperature, coolant flow and so on. SOC is a measure of how much charge that is left in the battery and it is an important parameter in estimating how much power that can be drawn from the battery. Another important parameter is SOH, it indicates the health of the battery since the battery capacity decreases over time. To determine SOH of the LIC, a good model of the battery ageing is needed. As this would require a lot of data SOH was not included in this thesis.

The battery pack is one of the most costly and heavy parts in an EV. Production of battery cells also contributes greatly to the increase of greenhouse gases, pollution of water and mineral resource depletion caused by EV:s [3]. Therefore it is very important to dimension the battery to make it as small as possible to reduce the strain on the environment, and the cost and weight of the EV.

SOH is highly dependent on the SOC window of which the Lithium Ion Cell (LIC) is operated [4]. To reduce the ageing process, the LIB is kept within a specified operation window, for example 20 – 80%. Because of the uncertainty of estimating SOC, the battery capacity has to be increased with the uncertainty. So if the SOC estimation has an accuracy of 5%, the battery is over dimensioned by 10% to compensate for this. If instead a more accurate SOC estimator would have been used, the battery capacity could have been used more efficiently, thus making the EV to have less impact on the environment.

1.2 Previous work

Extensive research has been performed around battery modelling, SOC estimations and BMS technology. Regarding SOC estimations especially interesting is [5] which has summarised a great many SOC estimation methods and rated their accuracy. It shows that the different methods vary in uncertainties but that by combining several SOC estimations the accuracy of the estimation is increased.

Many different BMS:s are available in commercial products. However since battery packs are heavy and bulky they are often custom designed for each application. This brings a need for custom designed BMS:s.

In 2010 when the all electric go-kart was first built at QRTECH AB, the master thesis "A Battery Management Unit" focused on designing the BMS for the system [6]. As the go-kart is being rebuilt as of spring 2018, a new LIB will be used which creates the need for a new BMS. There has also been advances in technology such as the Multicell Battery Monitor LTC6811-1 that was used in this thesis. The Multicell Battery Monitor shows great potential in managing the LIB.

1.3 Purpose

The purpose of this thesis is to develop a semi-distributed scalable BMS for an electric go-kart. Both hardware and software will be developed. The focus of this thesis would be on measurement and estimations of battery states.

2

Battery modelling and BMS theory

In Chapter 2 the theory for designing the BMS is presented. This includes theory about battery modelling, SOC estimation methods and passive battery balancing. The theory is later used in Chapter 3 and 4.

2.1 Battery modelling

In Figure 2.1 a schematic picture of a LIC can be observed. The battery consists of an anode and a cathode separated by an electrolyte. The electrolyte is electrically isolating but can conduct Li^+ -ions. When a load is connected to the battery, the electrons takes the path from the current collector on the anode side and are transported to the current collector on the cathode side. The Li^+ -ions are transported from the anode material to the cathode material through the electrolyte. There is a separator between the anode and cathode to protect the battery from short-circuit if the electrolyte is liquid [7].

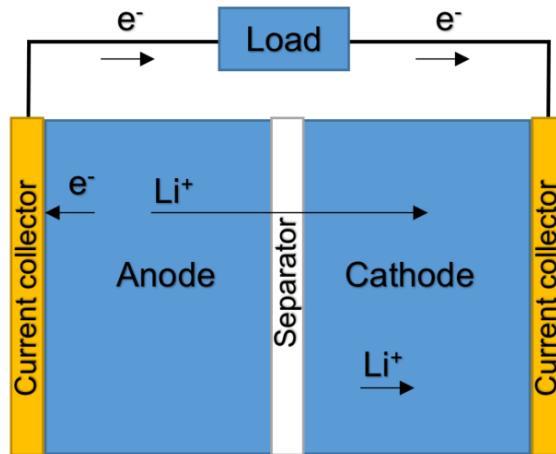


Figure 2.1: Schematic of a LIC when a load is connected. The electron and Li^+ -ion transportation from the anode to the cathode is indicated.

Depending on which materials that are used in the anode and cathode, the cell will have different characteristics [7]. The cells are usually limited by the cathode material, which sets the limits for the power and capacity of the cell [7]. Lithium

Iron Phosphate ($LiFePO_4$) is the cathode material used in this project. $LiFePO_4$ cells have a single-phase reaction when the cell has a high/low SOC level, resulting in a steep voltage increase/decrease at the edges of the voltage profile. During the rest of the voltage profile, the cell has a two-phase reaction, meaning that the voltage profile will have a flat appearance [7]. The advantage of this is that the cell will supply a stable voltage level to the load. However the flat voltage profile increases the difficulty to determine SOC. The voltage profile also shows a hysteresis behaviour, when the cell is charging the voltage is higher than when the cell is discharging. As a consequence of the hysteresis, capacity is lost during operation [7].

Compared to Lithium Cobalt Oxide ($LiCoO_2$) which is the most used cathode material today, $LiFePO_4$ has a lower power/capacity gain [7]. $LiFePO_4$ has other advantages such as being more safe to operate, if an object breaks the surface of the casing of a $LiFePO_4$ cell, no thermal reaction will occur. If the case is broken on a $LiCoO_2$ cell, and the materials are exposed to air or water, a thermal reaction will occur. Both the cathode materials are however sensitive to high temperatures above $300\text{ }^\circ\text{C}$ [7]. $LiCoO_2$ cells raises ethical questions as cobalt is mostly mined in the Democratic Republic of Congo where the working conditions in the mines are poor and child labour is not uncommon [8]. Neither lithium or cobalt are abundant materials on earth, and the increase of EV:s would increase the demand on the materials. As the recycling of lithium batteries is very poor, the usage of both materials will limit the occurrence of the materials for future generations and a great increase in prices are to expect in the future [9], [10], [11], [12].

The battery can be physically modelled with varying complexity and many modelling techniques have been proposed in literature. Since this project focuses on the BMS and not physical battery modelling, an equivalent and simplified circuit approach with two RC-links is taken to model the battery and can be seen in Figure 2.2 [13].

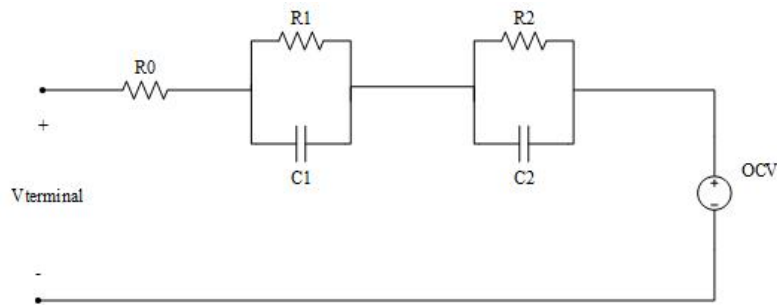


Figure 2.2: Equivalent circuit model of an LIC.

OCV can be seen in Figure 2.2 and is equal to the terminal voltage during no load operation. Depending on if the battery has been charged or discharge, the hysteresis curve has to be accounted for [7]. The terminal voltage ($V_{terminal}$) is the voltage where the load/charger is connected and is given by

$$V_{terminal} = OCV - R_0 I - I R_1 e^{-t/\tau_1} - I R_2 e^{-t/\tau_2} \quad (2.1)$$

where R_0 is the ohmic resistance, R_1 and R_2 are the polarisation resistances, C_1 and C_2 are the polarisation capacitances, I is the battery current, $\tau_1 = R_1 C_1$ and $\tau_2 = R_2 C_2$ [13]. R_0 in the model is defined as the resistance of the electrolyte and the connections to the battery [13]. The two RC-links are used to describe the nonlinear polarisation response [13]. To increase the accuracy of the model, more RC-links can be added. As the cell has different chemical reactions dependent on temperature, current, SOC and SOH, the battery parameters will vary with these.

2.2 BMS

The BMS needs to perform multiple functions for good operation of the battery. The BMS usually consists of a hardware part and a software part [5]. According to [5] the hardware can include sensor systems, safety circuits, charge control, thermal management and communications while the software part can include battery parameters, battery states (SOC, SOH), cell balancing, fault detection and a user interface [5].

According to [14] the main problems in BMS:s is firstly to get accurate cell voltage measurements. This is because of limited measurement accuracy and the high number of cells to be measured. Secondly to accurately estimate the battery states such as SOC, SOH etc. Thirdly to balance the cells since they charge at different rates and to different levels. The BMS needs to be able to perform these tasks and perform battery fault diagnostics.

2.3 SOC estimation methods

SOC indicates how charged the battery is, ranging from 0 % when the battery is fully discharged and 100 % when the battery is fully charged. $SOC(t)$ is defined as

$$SOC(t) = SOC(t_0) - \frac{100Q(t)}{Q_n} \quad (2.2)$$

where $SOC(t_0)$ is the initial SOC level, $Q(t)$ is the capacity that the battery is charged with and Q_n is the capacity when the battery is fully charged [15].

2.3.1 OCV method

The Open Circuit Voltage method (OCV method) is based on the nonlinear relationship between the OCV and SOC, $OCV = f(SOC)$ [5]. By knowing this relationship, SOC can be estimated if OCV is known. The OCV method can measure SOC with high accuracy if the EV is stationary for enough time, since the battery has to reach

equilibrium. This means that the battery has to rest from being charged/discharged for enough time for the OCV method to be accurate [5].

2.3.2 Coulomb counting method

The Coulomb Counting (CC) method is one of the most used SOC estimators since it is easy to implement [5]. It is defined as

$$SOC(t) = SOC(t_0) - \frac{100}{Q_n} \int_{t_0}^t \eta I(t) dt \quad (2.3)$$

where η is the coulombic efficiency and $I(t)$ is the measured battery current [5]. $I > 0$ means that the LIC is being discharged and $I < 0$ means that the LIC is being charged. In this project η is assumed to be 1. This method can however not measure $SOC(t_0)$, so for this function to work the starting capacity has to be known [5]. Discretizing (2.3) gives

$$SOC(k) = SOC(0) - \frac{100}{Q_n} \sum_0^n I(k) \tau \quad (2.4)$$

where n is the total number of samples and τ is the time period between samples.

2.4 Battery balancing

Since it is impossible to manufacture identical LIC:s, there is a problem with unbalanced cells in LIB:s [16]. When the LIC:s are produced they will have different capacity, internal impedance and self-discharge rate, causing them to be charged and discharged with slightly different rates and to different SOC levels [16]. This can cause the cells to be overcharged or undercharged and certain cells to spend a majority of there time in the high or low voltage range. This can lead to increased ageing and permanent damage to the cells [16].

A passive battery balancer using the controlled shunting resistor method can be used to limit the effect of unbalanced batteries by having a Transistor Switch (SW) in series with the discharge resistor (R_b) for each LIC [16]. By measuring the voltage over each LIC, the batteries can be balanced by controlling the SW individually to dissipate energy through R_b [16]. R_b can be dimensioned by setting

$$R_b = \frac{U_{max}}{I_b}, \quad (2.5)$$

where U_{max} is the maximum cell voltage and I_b the maximum discharge current [17]. The discharge current is selected such that the current is kept below the maximum current limited by the system, but high enough that imbalance will dissipate in a timely fashion as

$$I_b = \frac{\frac{SOC_{imbalance}}{100} Q_c}{t_b} \quad (2.6)$$

where $SOC_{imbalance}$ is the SOC imbalance, Q_c the nominal capacity [Ah] and t_b the time it should take to balance the cells [17].

3

Simulation set-up

Chapter 3 presents the simulation set-up of the battery model and the BMS that was built in Matlab®Simulink®. The BMS model was code generated into C which where uploaded to the Electric Control Unit (ECU) and later used in Chapter 4.

The setup orientates around the BMS which receives its inputs from an analogue charge and discharge circuit with a battery model, a simple load case setup and a battery balancing circuit. The battery model consists of 16 identical series connected battery cell models which is described in Section 3.1. Figures of the simulation set-up can be found in Appendix A.

3.1 Battery cell model

The battery cell model was based on Figure 2.2. The battery parameters R_0 , R_1 , R_2 , C_1 , C_2 were taken from measurements, see Table 6.2. The OCV was implemented as a two dimensional look-up table based on the data from the cell characterisation seen in Figure 6.5 using a simplified version of (2.1). By using the current applied by the Gamry instrument during the measurement and a resistance approximately equal to $R_0 + R_1$ for 25, 30 and 45°C, see Table 6.2, the voltage drop caused by the small current was removed from the data. SOC and temperature were used as breakpoints and the corresponding voltage as output. To provide a SOC input to the lock-up table, CC was used with perfect parameters for each cell separately.

3.2 BMS model

The BMS model was given the measurement values of I , $V_{terminal}$ and T to manage the LIB. Enable Equalising is also given to the system to determine when the passive battery balancing should occur. The outputs of the BMS were $V_{terminal}$, I , SOC , T , Gate signals (S), and over/under detection of voltage, temperature and current. An overview of the BMS can be seen in Figure 3.1.

3.2.1 SOC estimators

Three methods were used to estimate SOC. The first method, SOC_{OCV} only used the OCV method to estimate SOC. The OCV method implements a inverse version

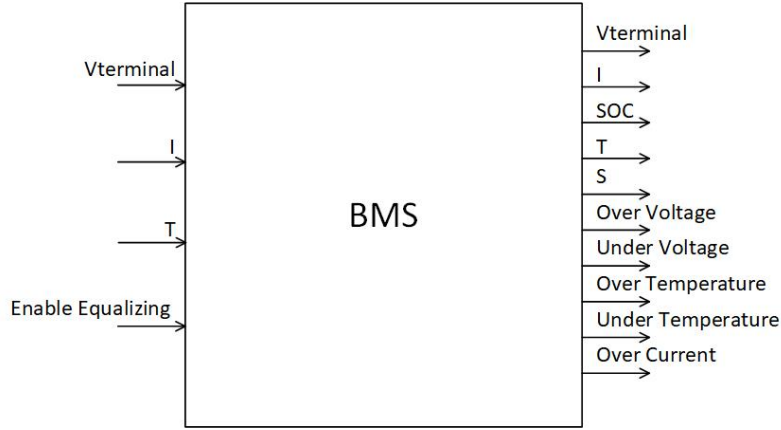


Figure 3.1: Overview of the BMS. With $V_{terminal}$, I , T and Enable Equalising, the BMS manages the system.

of the lock-up table used in the Battery model in Section 3.1. Here voltage and temperature are used as breakpoints and the corresponding SOC level as output.

The second and third methods, SOC_{CC} and $SOC_{CCedges}$ both used a combination of both the CC and the OCV method. The CC method is based on (2.4) with $\tau = 100 \text{ ms}$. If $I < 0$, the LIB is charging and if $I > 0$, the LIB is discharging. The CC method and the OCV method cooperated as shown in Figure 3.2. When $I = 0$ for more than 30 minutes, the OCV method is used to estimate a new $SOC(0)$ and the integration were reset. When $I \neq 0$ the CC method is used instead. The CC method causes the SOC estimation to drift as the measuring error is accumulated, the OCV method compensates for this since the SOC is reset by the OCV method. $SOC_{CCedges}$ only used the OCV method when $V_{terminal} > 3.4 \text{ V}$ or $V_{terminal} < 3.1 \text{ V}$. This method was implemented to avoid SOC estimation based on the flat region of the voltage curve.

3.2.2 Battery balancing

The battery balancing in the BMS model is responsible for setting the gate signal S_x controlling the SW_x to discharge the cells as described in Section 2.4. To determine if the LIC needs to be balanced, a voltage tolerance of 0.05 V was set. If the LIC was 0.05 V higher than the average cell voltage, S_x was set high, if not S_x remained low. To make sure that the voltage measurement was not done while the battery balancing was active, a clock pulse with a time period of 100 ms was inserted.

3.2.3 Fault detection

When an under- or overvoltage is detected by the system, a signal should be sent to the relays to disconnect the system. This is done by comparing the highest and the lowest cell voltages to the maximum and minimum voltage levels allowed. If the cell voltages are in the allowed range, the signal goes high, if they are not the

signal goes low and the relays are activated. A similar approach is done to see if the batteries are operated within the allowed temperature and current range.

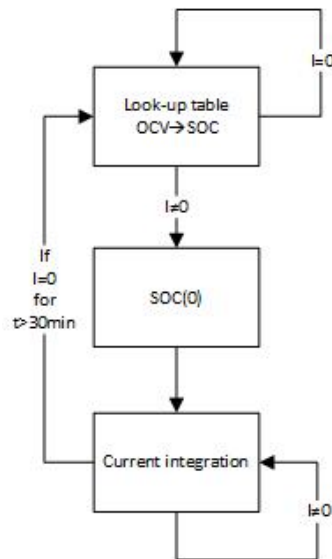


Figure 3.2: Simulation set-up of the OCV and the CC methods. The OCV method consists of a look-up table and the CC method consists of current integration. If $I = 0$ for longer than 30 min, the OCV method applies, otherwise the CC method is active.

4

BMS Design

Chapter 4 presents the BMS design. This includes the go-kart specifications and a description of the designed hardware and software for the BMS. The evaluation of the design can be found in Chapter 6.

4.1 Go-kart specification

The LIC:s intended for the go-kart is the Headway 40152S cells, see Appendix C. 16 of these cells in series and two in parallel can supply the go-kart with 51.2 V, an average current of 100 A and a peak current of 200 A. However, these cells did not arrive within the time frame of the project, instead the A123: HTPFR18650-1100mAh-3.2V cells were used for testing and tuning the BMS system, see Appendix D. The specifications of both battery packs are shown in Table 4.1. The BMS was designed for the Headway 40152S cells but all simulations, measurements and tests in the report are based on the A123: HTPFR18650-1100mAh-3.2V cells.

Table 4.1: Specification for the battery pack intended for the go-kart and the one for testing of the BMS.

	Go-kart LIB	Testing LIB
Nominal voltage	51.2 V	51.2 V
Nominal capacity	1440 Wh	56.32 Wh
Min cell voltage	2 V	2 V
Nominal cell voltage	3.2 V	3.2 V
Max cell voltage	3.6 V	3.65 V
Rated charge current	90 A	5 A
Rated discharge current	150 A	33 A
Max discharge current	300 A (30 s)	40 A (10 s)
Drive time	15 min	-
Number of cells in series	16	16
Number of cells in parallel	2	1
Weight	17.3 kg	0.356 kg
Cell dimension dia x h	40 x 165.5 mm	18.2 x 65.2 mm
Max temperature	45	60
Min temperature	-20	-20

4.2 Hardware

The hardware was designed in Altium. Figure 4.1 shows how the system was implemented. The multicell battery monitor LTC6811-1 [17] was used to measure the terminal voltages of the 16 LIC:s and perform 10 temperature measurements. To enable voltage measurement on 16 LIC:s, two LTC6811-1:s were used. The two LTC6811-1:s were connected in a daisy-chain configuration with a 2-wire isolated interface. To enable this configuration, a isoSPI Isolated Communications Interface LTC6820 [18] were used. The LTC6820 converts the 4-wire SPI system to a 2-wire isolated interface, isoSPI. The QRx was the ECU of the system and was provided by QRTECH AB. The QRx contained the BMS software that controlled the system. The current was measured with a LEM current transducer DHAB S/118 [19] that was connected to an ADC on the QRx. To log the data during operation a PC was connected to the QRx via a CAN bus.

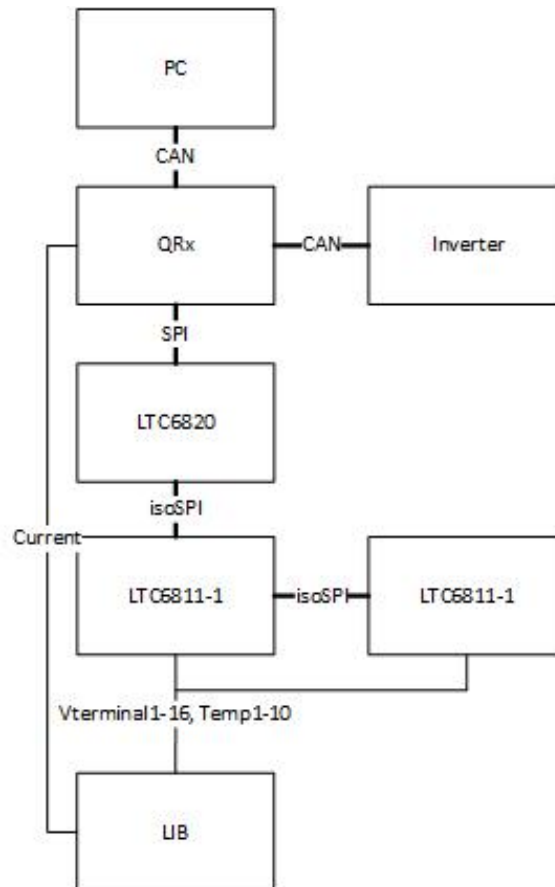


Figure 4.1: System flow chart. Shows how the LIB, LTC6811-1, LTC6820, QRx, inverter and computer are connected.

A picture of the design can be seen in Figure 4.2 the turquoise areas in the figure shows the 16 series connected LIC:s, the red areas shows the PCB:s with LTC6811-1, the purple area shows the QRx and the PCB with LTC6820, and the grey area shows the CAN transceiver.

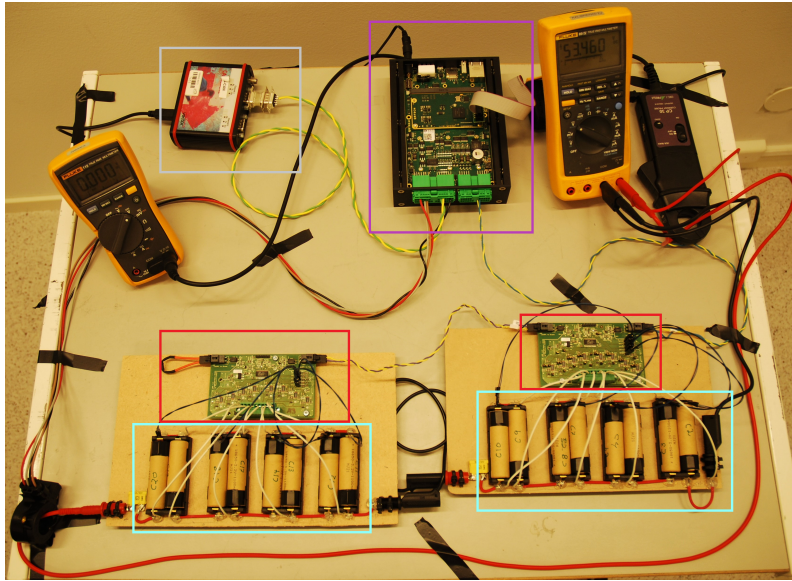


Figure 4.2: The implemented design. The 16 cells are in the blue areas, the PCB:s with the LTC6811-1 are in the red areas, The QRX and the PCB with LTC6820 are in the purple area and the CAN transceiver is in the grey area.

LTC6811-1 was placed on a PCB that can be seen in Figure 4.3. The PCB were heavily based on a design made by QRTECH AB but modified to fit this project. In the pink area, the LTC6811-1 can be seen with the components used for configuration of the LTC6811-1 [17]. The blue area shows the power supply to the LTC6811-1, the circuit is supplied with the total voltage of all cells and via a linear regulator, 5 V is also supplied to the circuit. The yellow area shows the communication circuits and the connections. The green area shows one of the battery balancing circuits that is further introduced in Section 4.2.4. The grey area shows the temperature measuring circuit that is further introduced in Section 4.2.2.

The PCB with LTC6820 can be seen in Figure 4.4, it was designed by QRTECH AB and used in this project [18]. LTC6820 is shown in the green area. The PCB was connected to the QRx via an extended circuit also provided by QRTECH AB.

4.2.1 Voltage measurement

The LTC6811-1 has ADC:s that measures the 16 terminal voltages with a measurement accuracy of 1.2 mV, however the system contributes with additional measurement errors as the data is shifted in the communication interface etc.

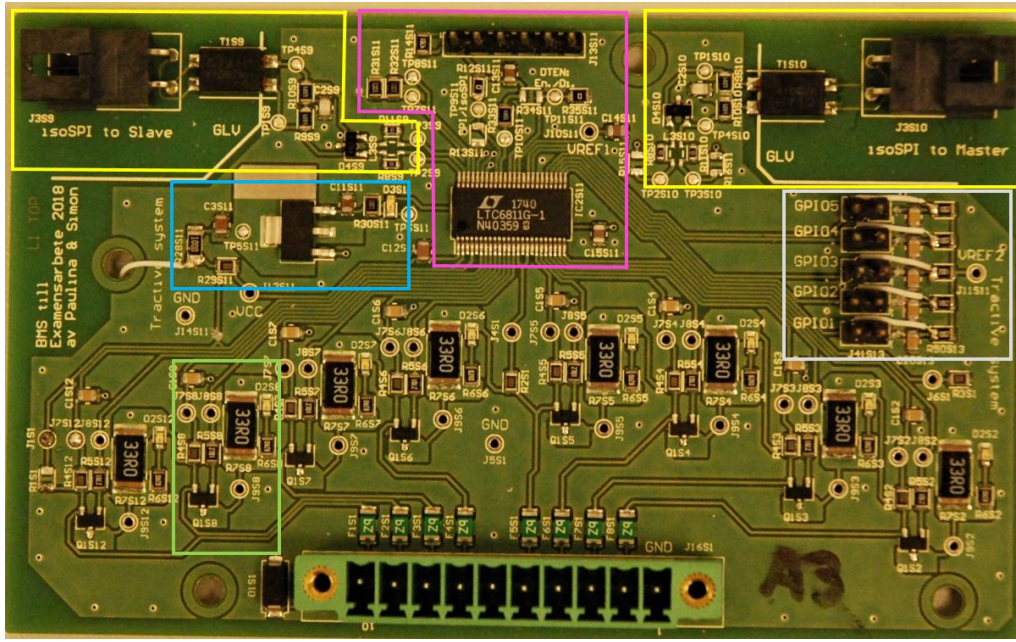


Figure 4.3: The PCB with the LTC6811-1. The pink area shows the LTC6811-1 and its configuration settings. The blue area shows the power supply to the LTC6811-1. The yellow area shows the communication circuits and their connections. The green area shows one of the battery balancing circuits. The grey area shows the temperature measuring circuit.

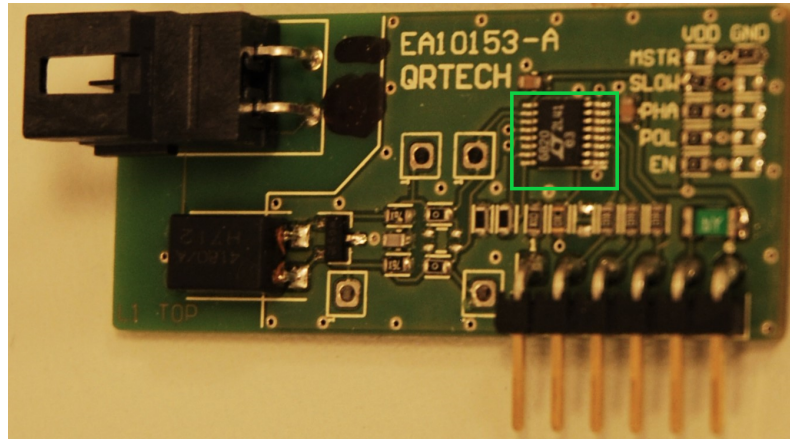


Figure 4.4: The PCB with the LTC6820. LTC6820 is shown in the green area

4.2.2 Temperature measurement

The 10 GPIO ports of the two LTC6811-1:s are used to measure the temperature. The termistors used to measure the temperature are the NXFT15XH103FA2B025 termistors [20]. They have a range of $-40\text{ }^{\circ}\text{C}$ to $125\text{ }^{\circ}\text{C}$ and has a resistance tolerance of 1 %. Figure 4.5 shows the temperature measurement circuit. A voltage divider is used to measure the voltage (V_{temp}) over the termistor which has a variable resistance (R_{temp}) depending on the temperature. The voltage reference (V_{REF2}) is measured by the QRx and has a nominal value of 3 V and the reference resistor (R_{REF}) is

equal to $10\text{ k}\Omega$. This gives

$$R_{temp} = R_{REF} \frac{1}{\frac{V_{REF2}}{V_{temp}} - 1} \quad (4.1)$$

(4.1) can be used to calculate the temperature T as

$$T = \frac{1}{\frac{\ln(R_{temp}/R_{REF})}{B} + \frac{1}{T_{REF}}} \quad (4.2)$$

where T_{REF} is 298.15 K , and B is 3380 K .

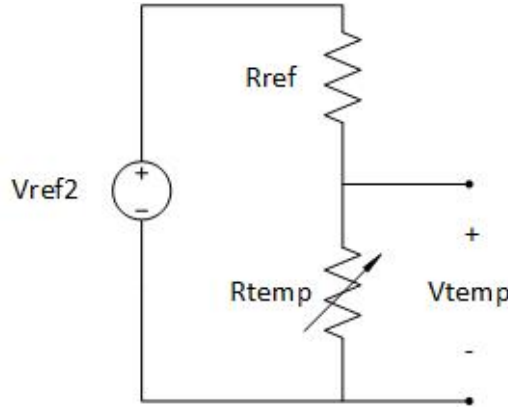


Figure 4.5: Temperature measurement circuit. A voltage divider is used to measure the voltage over a termistor.

4.2.3 Current measurement

To measure I the LEM current transducer DHAB S/118 was used. It is a open loop transducer using the hall effect to measure current. It has two channels, channel 1 to measure $\pm 30\text{ A}$ and channel 2 to measure $\pm 350\text{ A}$ with a resolution of 2.5 mV . The accuracy varies between $0.15 - 0.83\text{ A}$ for channel 1 and $1 - 6.7\text{ A}$ for channel 2, depending on the current and the temperature. I can be calculated as

$$I = \left(\frac{5}{V_c} V_I - V_0 \right) \frac{1}{G} \quad (4.3)$$

were V_c is the supply voltage equal to 5 V , V_I is the output voltage from the LEM current transducer, V_0 is the offset voltage equal to 2.5 V and G is the sensitivity equal to 66.7 mV/A for channel 1 and 5.7 mV/A for channel 2.

4.2.4 Battery Balancing

Figure 4.6 shows the battery balancing circuit. By choosing I_b to 133 mA , and knowing that Q_c is 20 Ah the discharge time could be calculated to 9 h with (2.6) which was deemed appropriate for the application. Since U_{max} of the cells was 3.65 V , the total discharging resistance, R_b , could be calculated to $27,4\text{ }\Omega$ with (2.5). To make it easier to test and debug the system a light emitting diode was

placed in parallel with the discharge resistor. To limit the current through the diode but keep R_b close to its original value R_{b0} was selected as $33\ \Omega$ and R_{b1} as $82\ \Omega$. To filter the voltage measurement ($V_{TerminalMeas}$) an RC circuit was used. The filter resistor (R_f) was $100\ \Omega$ and the filter capacitor (C_f) was $10\ nF$ as recommended in [17]. The transistor (SW_X) had a gate resistance (R_g) of $2.7\ k\Omega$.

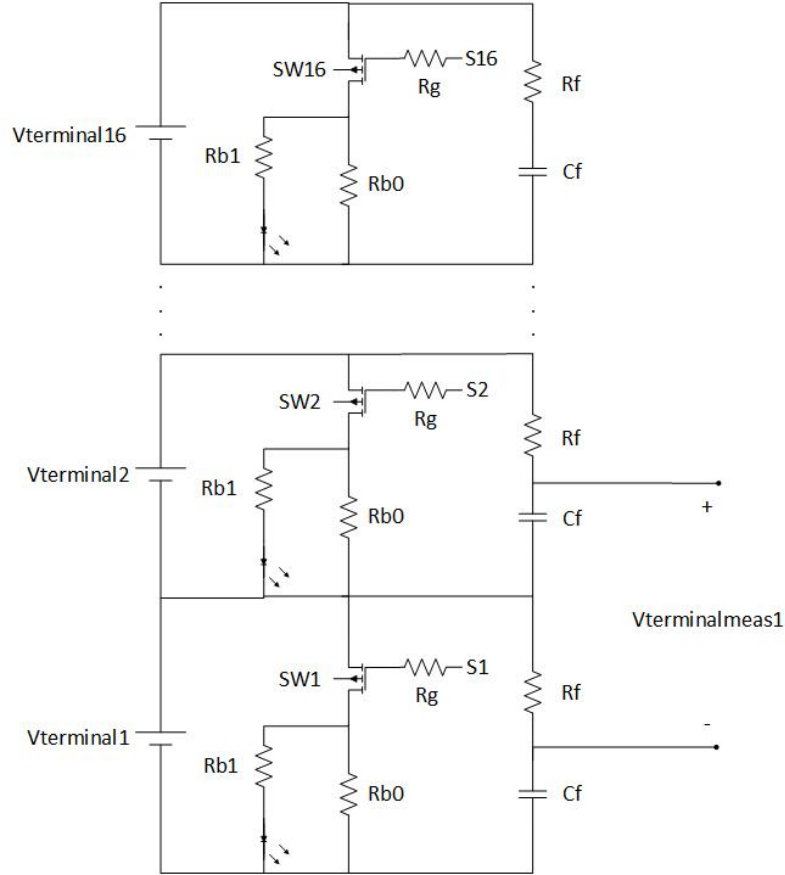


Figure 4.6: The design of the battery balancer.

4.2.5 Communication

The QRx controls the LTC6811-1 via SPI that is converted to isoSPI with the LTC6820 circuit. The SPI communication is constructed with 4-wires as in Figure 4.7. The QRx is the SPI master and the LTC6820 the SPI slave. The communication interface is enabled when SS is pulled low, and disabled when SS is pulled high. The clock signal SCK is supplied from the QRx and set to 70 kHz . Instructions are sent from the master to the slave via MISO, that shifts the information out from the QRx bit by bit with the speed of the clock signal. The same process occurs when the slave sends instructions to the master, but instead the MISO connection is used.

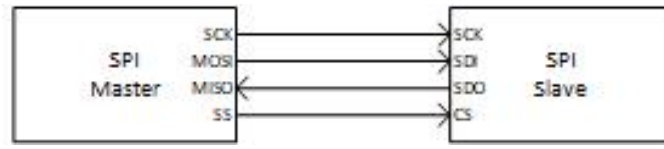


Figure 4.7: SPI communication.

The daisy-chain communication interface can be seen in Figure 4.8. It shows how the QRx, LTC6811-1 and LTC6820 are connected. The QRx and the LTC6820 are connected as in Figure 4.7. LTC6820 sends communication to LTC6811-1 via isoSPI. The isoSPI communication consists of two wires, IP (positive) and IM (negative). By sending pulses with varying length and sign, the bits are shifted through the communication chain and interpreted by LTC6811-1 [17], [18].

4.3 Software

The BMS software was code generated from the Matlab®Simulink®model and implemented together with additional C code in Actric Studios Autosar environment. The description of the BMS software can be seen in Section 3.2.

After every 100 ms , the QRx sends commands to the LTC6811-1:s via SPI, to start voltage measurements on all the cells, temperature measurements on all sensors and a status check on the LTC6811-1 itself. If the battery balancing is activated, the appropriate gate signals are sent to the battery balancing circuit as well. The commands used are listed in Table 4.2, between every write command, a delay of 5 ms was set. To interpret the temperature, (4.1) and (4.2) were used. The ADC is read on the QRx to make a current measurement and with (4.3), I is calculated. If $|I| < 30\text{ A}$ the measurement from channel 1 of the LEM current transducer is used, if not the measurement channel 2 is used. The measurements become inputs to the BMS software that sends the outputs via CAN to a PC where the data is logged.

Table 4.2: Commands used to write and read measurements on LTC6811-1 [17].

Command	Description	Binary code
Wake up	wakes the LTC6811-1/isoSPI	1111 1111 1111 1111
ADCV	Write Cell Voltage ADC Conversion	0000 0011 0110 0000
ADAX	Write temperature ADC Conversion	0000 0101 0110 0000
ADSTAT	Write status check of LTC6811-1	0000 0101 0110 1000
RDCVA	Read cell voltage register A	0000 0000 0000 0100
RDCVB	Read cell voltage register B	0000 0000 0000 0110
RDCVC	Read cell voltage register C	0000 0000 0000 1000
RDCVD	Read cell voltage register D	0000 0000 0000 1010
RDAUXA	Read temperature register A	0000 0000 0000 1100
RDAUXB	Read temperature register B	0000 0000 0000 1110
RDSTATA	Read status register A	0000 0000 0001 0000
WRCFGA	Write configuration register, additional	0000 0000 0000 0001
	data with gate signals were sent as well	

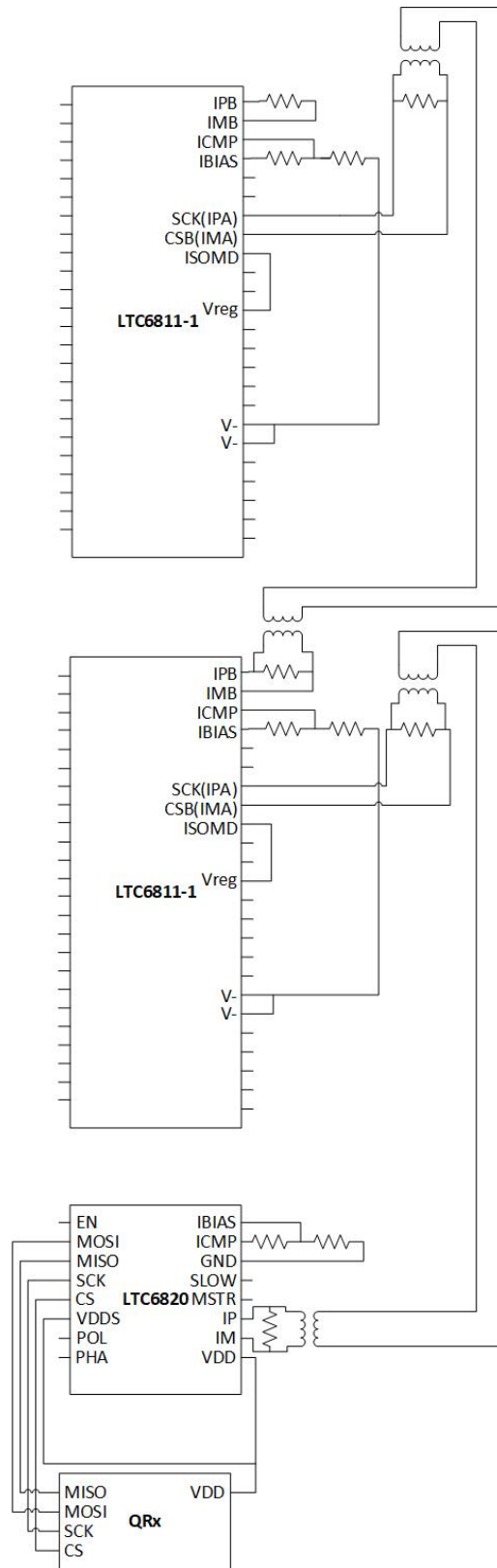


Figure 4.8: Transformer isolated daisy-chain communication configuration between the QRx, LTC6820 and the two LTC6811-1:s.

5

Measurement set-up

Chapter 5 presents information on how the measurements were set-up. This includes measurements to extract the LIC:s parameters and characterisation, also measurements to verify operation of the BMS. The results from the measurements are presented in Chapter 6.

5.1 Battery parameter extraction

To extract the battery parameters, R_0 , R_1 , C_1 , R_2 and C_2 a Electrochemical Impedance Spectroscopy (EIS) test was preformed with a Gamry Reference 3000. The instrument was calibrated before the tests started. The test setup can be seen in Figure 5.1, The cell was connected to the Gamry instrument via a four-terminal sensing setup. The four-terminal sensing setup consists of two wires to carry the current and two wires for the voltage sensing, the method was used to increase the accuracy of the measurements. A frequency sweep was done over the cell when the SOC was 50 %. By plotting the measurement values in a Nyqvist curve, the parameters could be estimated. The same measurement setup was used to find the OCV curve of the LIC:s.

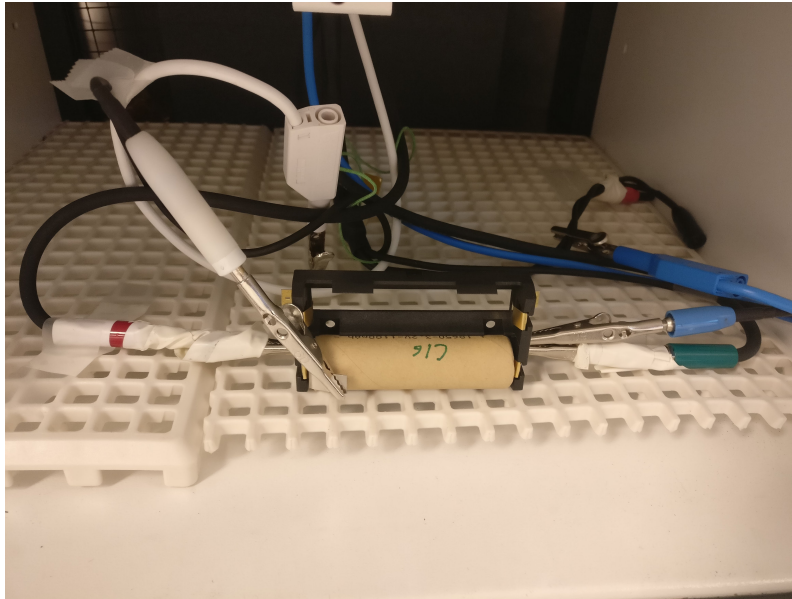


Figure 5.1: Measurement set up for extracting the battery parameters and the OCV curve. Here cell 16 is shown in the temperature chamber.

5.2 BMS verification

To validate the performance of the BMS, different discharge and charge test were performed on the LIB, the measurement setup can be seen in Figure 5.2. As a safety precaution, the test were preformed in an physically and electrically isolated room. The cells was also covered with a plexiglas, to reduce the risk of accidentally short circuiting the cells. The instruments used and their accuracy are listed in Table 5.1. Before the start of the test, a reference voltage measurement on the LIB was taken with a FLUKE 89 4 TRUE RMS MULTIMETER. During a discharge test the Electronic Load EA-EL 9400-50 HP was used as a load and was connected in series with the LIB. If instead a charge test was performed, the Power supply EA-PS 2042-06B was used to charge the LIB. A GMC-I Prosys CP- 30 Multimeter Current Clamp Adapter was used to measure a current reference during the charge/discharge. After the test, the LIB remained stationary for 1 hour and than an additional voltage reference measurement was taken with the FLUKE 89 4 TRUE RMS MULTI. The voltage references was compared to the SOC level indicated with the BMS to verify the performance of the BMS.

Table 5.1: The instruments used to verify the performance of the BMS and their accuracy.

Instrument name and model	Accuracy
FLUKE 89 4 TRUE RMS MULTI.	$0.03\% + 3 \text{ mV}$
GMC-I Prosys CP- 30 Multimeter Current Clamp Adapter	$1\% + 2 \text{ mA}$
Power supply EA-PS 2042-06B	$< 0.2\%$
Electronic Load EA-EL 9400-50 HP	Voltage $< 0.2\%$
	Current $< 0.1\%$

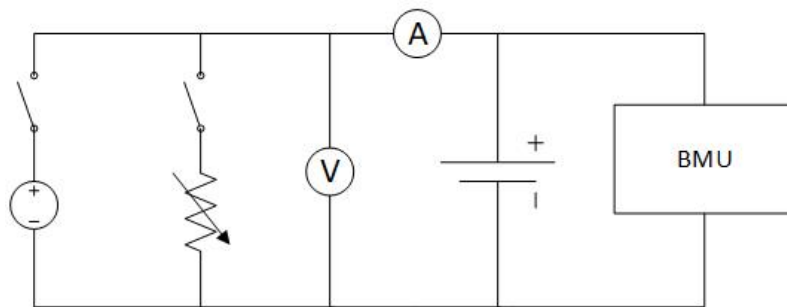


Figure 5.2: Circuit diagram of the BMS verification. Depending on if a charge or discharge test was preformed, a DC source or an electronic load was connected.

6

Analysis of the BMS

In Chapter 6 the analysis of the BMS is presented. Firstly the Cell parameters and characteristics are analysed regarding deviation and temperature dependence. Secondly are the SOC estimations in the BMS analysed regarding accuracy.

6.1 Cell parameters and characteristics

Charge and discharge tests were performed with 0.1C with the goal to extract the OCV curves of the LIC:s. The 20 cells available were numbered from 1-20 (Cell 1-20). To study the variations between the cells three different cells were tested. Cell 1, 6 and 16, and are compared in Figure 6.1 and 6.2. To study the OCV dependence on temperature, two additional tests were conducted on cell 16 inside a temperature chamber and the result is displayed in Figure 6.5. Finally, the cell parameters R_0 , R_1 , C_1 , R_2 and C_2 were extracted for different temperatures using an EIS test and the result can be seen in Figure 6.8.

6.1.1 OCV

In Figure 6.1 the charge and discharge curves with 0.1C are shown for three different battery cells at 25 °C. Cell 1 (black), with the charge cycle shown with a solid line and the discharge cycle shown with a dashed line. With a similar manner, cell 6 (red) and cell 16 (blue) are shown. In the figure it can be seen that the curves follows the characteristic shape of $LiFePo_4$ cells described in Section 2.1. It can be seen that a rapid voltage change occurs between the SOC intervals 0 – 10% and 95 – 100%, and a very small voltage change occurs between the SOC intervals 10 – 95%.

In Figure 6.2, a zoomed version of Figure 6.1 is displaying SOC between 10 – 100%. The figure shows that during the majority of the SOC window the voltage changes with $\sim 200\text{ mV}$. This makes it necessary to have very accurate voltage measurements from the BMS to be able to use the OCV method for SOC estimations. Also, a slight deviation between the cells can be observed. This deviation can be further studied in figure 6.3 and 6.4 which show the deviation from the average of all three cells for charge and discharge at 25 °C. It can be observed that the deviation is small in most of the SOC window but increases for both low and high SOC levels.

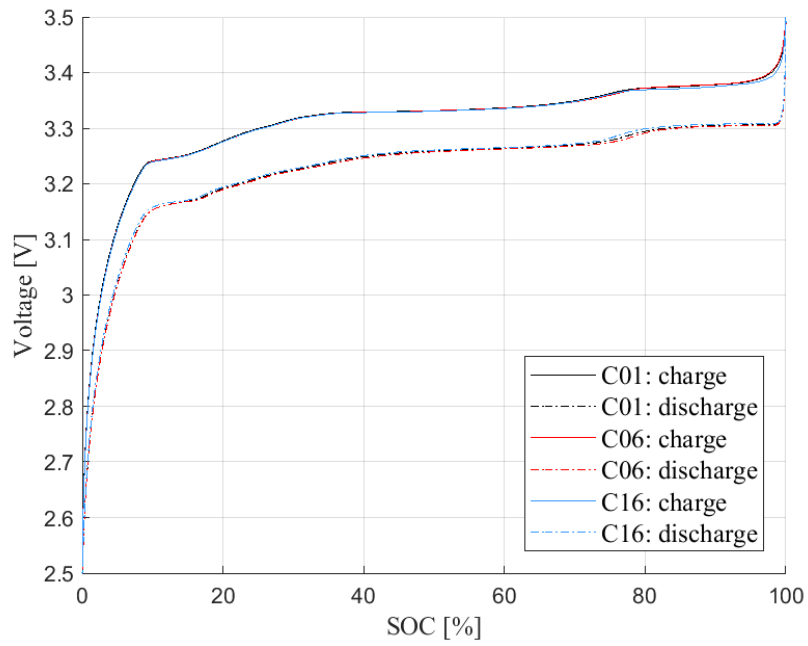


Figure 6.1: Voltage profile of charge and discharge at 0.1C for three different cells.

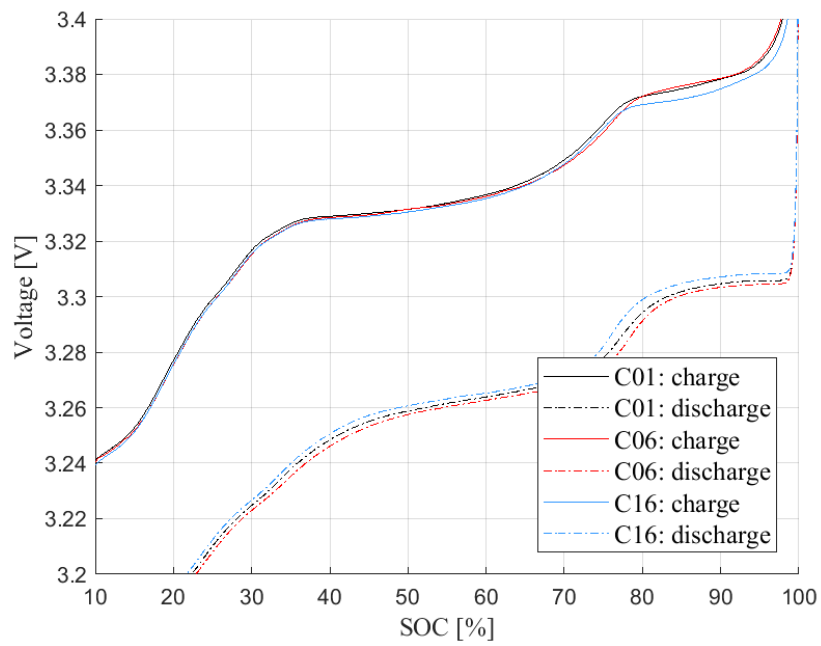


Figure 6.2: Voltage profile for SOC between 10 – 100% of charge and discharge at 0.1C for three different cells.

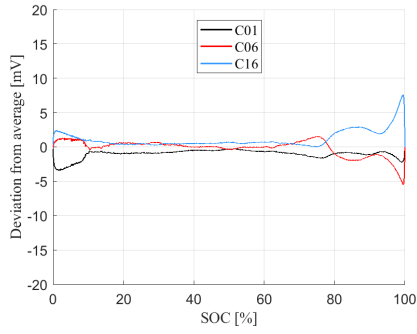


Figure 6.3: Deviation from average at charge between the different cells at 25°C.

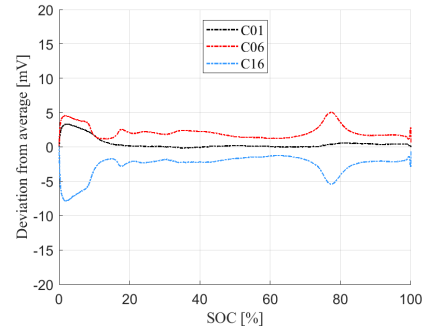


Figure 6.4: Deviation from average at discharge between the different cells at 25°C.

Figure 6.5 shows the charge and discharge curves of cell 16 for 25, 30 and 44 °C. These temperature values were chosen to fit the expected temperatures of the cells during testing of the system. As different LIC:s will be used in the real go-kart, the real cell temperature during operation was not included. The cycle with 25 °C (black) is showed with the charge cycle as full line and the discharge cycle as a dashed lined. With a similar manner, the cycle with 30 °C (red) and the cycle with 44 °C (blue) is showed. Similar to Figure 6.3 and 6.4 the deviation from the average of the three temperatures can be observed in Figure 6.6 and 6.7 for charge and discharge. The figures show that the deviations are more pronounced between the different temperature then to the different cells. The deviations are greater for high and low SOC compared to SOC between 20 – 80 %. During discharge the deviations are approximately constant over the entire SOC window. When comparing Figure 6.3 and 6.4 to Figure 6.6 and 6.7 it is clearly shown that the OCV is more dependent on temperature than on the deviations between the cells, therefore temperature is taken into consideration when designing the SOC estimators.

6.1.2 Energy content

During the cell characteristic measurements, two charge and two discharge cycles were performed in each test. The energy content in the LIC:s were calculated by integrating the current applied by the Gamry instrument during cell characteristic and the result is displayed in Table 6.3. It can be observed that Q_n differ between the LIC:s and for different temperatures. However for simplicity, the mean value of the average column in the table was calculated to $Q_n = 1.076Ah$. This value was implemented in the CC models and simulations. As Q_n increases with temperature, this could have resulted in an overestimation of Q_n .

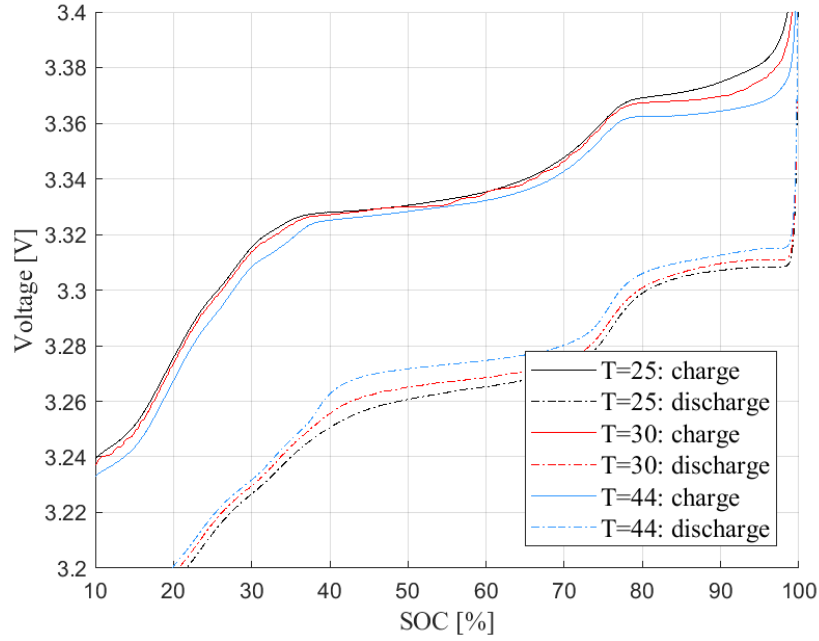


Figure 6.5: Voltage profile for SOC between 10 – 100% of charge and discharge at 0.1C for three different temperatures.

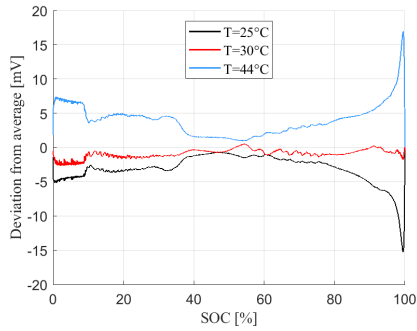


Figure 6.6: Deviation from average at charge between the different temperatures for C16.

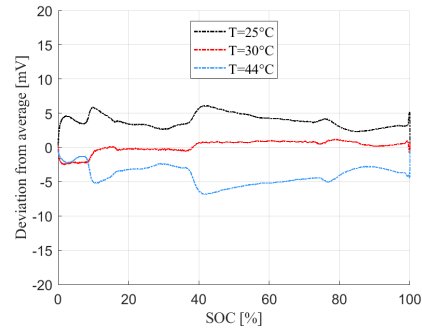


Figure 6.7: Deviation from average at discharge between the different temperatures for C16.

Table 6.1: Calculated energy content in the cells. The average Q_n was calculated to 1.076Ah by taking the average of the average column.

	Discharge 1	Discharge 2	Charge 1	Charge 2	Average
C01 : 25°C	1.077 Ah	1.080 Ah	1.079 Ah	1.079 Ah	1.079 Ah
C06 : 25°C	1.078 Ah	1.078 Ah	1.074 Ah	1.074 Ah	1.074 Ah
C16 : 25°C	1.049 Ah	1.062 Ah	1.057 Ah	1.057 Ah	1.057 Ah
C16 : 30°C	1.084 Ah	1.085 Ah	1.085 Ah	1.085 Ah	1.085 Ah
C16 : 44°C	1.085 Ah	1.087 Ah	1.086 Ah	1.086 Ah	1.086 Ah

6.1.3 EIS

The Nyquist plot for the EIS measurements are shown in Figure 6.8. The EIS measurements were swept from 1 Hz to 2.5 kHz at 50 % SOC for 25 °C (black), 30 °C (red) and 44 °C (blue). The measured impedance (z_{meas}) is shown with stars. The corresponding RC link models, is seen with dashed lines in the figure with the parameters as described in (6.1) and (6.2).

The impedance characteristics of R_0 and the two RC chains from Figure 2.2 are expressed in the Laplace domain as

$$Z(R_0, R_1, C_1, C_2, R_2) = R_0 + \frac{R_1}{sR_1C_1 + 1} + \frac{R_2}{sR_2C_2 + 1} \quad (6.1)$$

The Matlab® function *fminsearch()* was used to minimise the error between $Z(R_0, R_1, C_1, C_2, R_2)$ and the measurements (z_{meas}) as

$$err(R_0, R_1, C_1, C_2, R_2) = \text{sum}(\text{abs}(Z(R_0, R_1, C_1, C_2, R_2) - z_{meas})). \quad (6.2)$$

The result from *fminsearch()* are displayed in Table 6.2 and plotted in Figure 6.8 using (6.1) to compare to the measured data. In the figure it can be seen that the measured values and the fitted curve differ, which result in estimation errors. To increase the accuracy of the battery model, more RC-links can be added, which should result in a better parameter fit. Also the battery parameters varies with SOC, SOH and current. For this application it was determined that more accurate parameters were not necessary and it is assumed that the parameters only vary with temperature. This will yield a uncertainty in the the OCV look-up table when comparing the simulations to the real measurements.

Table 6.2: Battery parameters R_0 , R_1 , C_1 , R_2 and C_2 extracted from the EIS test for 25, 30 and 44 °C.

Parameter	25 °C	30 °C	44 °C
R_0 [mΩ]	23.9	22.7	22.6
R_1 [mΩ]	12.6	8.9	3.2
C_1 [F]	0.307	0.309	0.815
R_2 [mΩ]	8.0	8.2	4.8
C_2 [F]	166.6	187.4	282.2

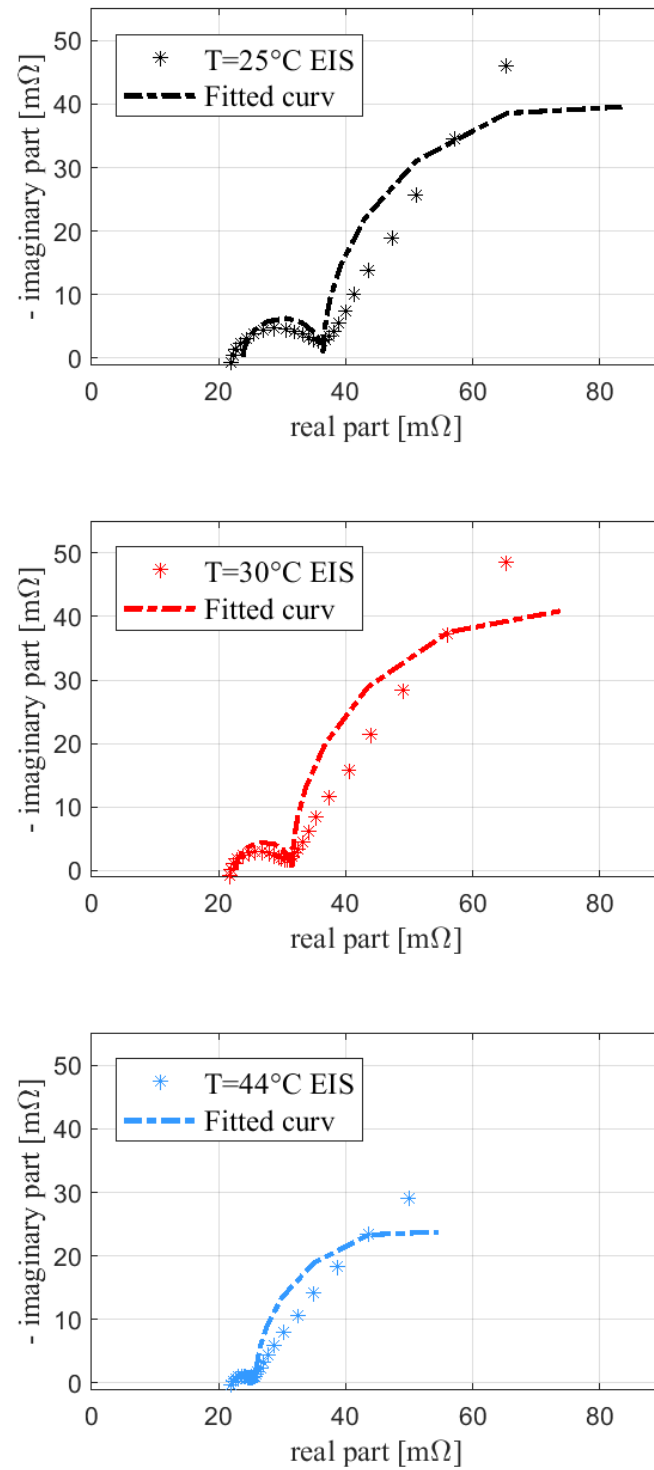


Figure 6.8: Comparison of EIS measurements and parameter fit for different temperatures.

6.2 SOC estimation verification

A discharge test was performed to evaluate the SOC estimation methods. I (blue) is displayed in Figure 6.9 the test consisted of five discharge pulses. First three discharges with 5C for $\sim 3 \text{ min}$, then a discharge with 5C for 1.33 min and 2C for 1.33 min , and lastly a discharge with 0.5C for 2.17 min . The LIB was left stationary for $\sim 1 \text{ h}$ after each discharge for V_{terminal} to stabilise.

The noise in Figure 6.9 is in line with the measurement error of the transducer and the ADC in the QRx. To reduce the noise, one could have taken several current measurements and use the average to measure the current. Also the data in the figure show that there is a zero current offset of -11.9 mA and when discharging at 5C a measurement offset of -261 mA . This indicates that the calibration of the current transducer is off and that further calibration is needed. It also indicates that the offset varies with current, thus making an algorithm for the behaviour is needed.

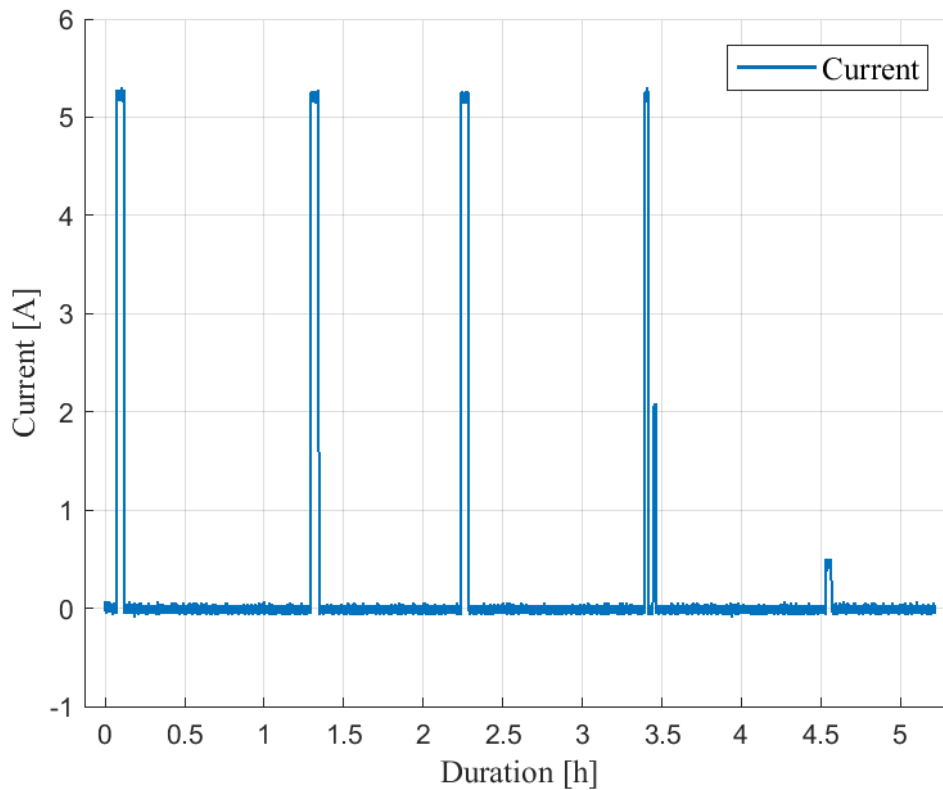


Figure 6.9: I during the discharge test to evaluate SOC estimation methods

Figure 6.10 shows V_{terminal} of the 16 LIC:s during the discharge test. The figure displays that during discharge, the voltage reduces rapidly, and is almost stabilised after 0.5 h . The cells keeps decreasing after 0.5 h but the decrease is so small that the effect can be neglected for this application. The small decrease could be that the cell have not had time to fully stabilise or that the BMS hardware is consuming

enough power to make an impact on the voltage. The variation of the LIC:s can also be seen. During discharge, the voltages are reduced to different levels, which indicates variation in the battery parameters among the cells. The cells also show great variations during high and low SOC, this indicates variations in capacity, resulting in that the cells are charged and discharged with different speeds. After 5.2 h, the highest charged cell has a $V_{terminal}$ of 2.85 V and the lowest charged cell has a $V_{terminal}$ of 2.66 V. This shows larger variations in OCV than estimated in Figure 6.4. Also interesting is that the cell with the highest voltage in the high SOC region (dashed light blue) has the second lowest voltage in the low SOC region. This indicates that the capacity variance is large for this cell compared to the other LIC:s.

In Figure 6.10 more than 12 million measurements are represented, among these the QRx also received 52, zero voltage measurements, i.e. 52 data sets were lost. This is not represented in the figure. Since there is no filter on the input data to the BMS this problem propagates to the SOC estimations and especially the OCV method. However, since only 4.3 measurements are lost per 1 million samples the affect on the SOC estimations are negligible. For the purposes of this report and to make the data less cluttered, the outliers have been filtered out from the affected figures in the report but can be seen in Appendix B. Although this is acceptable for the SOC estimations this will cause the over and under voltage detection to send CAN messages that should stop the inverter and turn the car off. This has to be addressed before implementing the BMS in the car.

Figure 6.11 shows SOC estimations during the discharge test. SOC is estimated with three methods, SOC_{OCV} (blue), SOC_{CC} (red), and $SOC_{CCedges}$ (yellow - -) as described in Section 3.2.1 and compared to a manual calculation of SOC ($SOC_{ManCalc}$) (black). $SOC_{ManCalc}$ is calculated based on the reference current measured with a current clamp, the values can be seen in Table 6.3 using (2.3). It can be observed that the three estimations methods deviate both from each other and from $SOC_{ManCalc}$ which is used as a reference.

Table 6.3: Result from current clamp and the electric load setting during the active periods of the discharge test.

Pulse	Duration [s]	Electric load setting [A]	Current clamp [A]
1	195.3	5.5	5.48
2	180.5	5.5	5.48
3	180.6	5.5	5.49
4.1	80.3	5.5	5.49
4.2	81.3	2.2	2.2
5	129.5	0.55	0.55

At the start of the discharge test, one can see that the SOC estimations all start at 100 % as a result of using the OCV method to calibrate against. During the first discharge pulse SOC_{OCV} is drastically lowered as a result of the lowered $V_{terminal}$ as can be seen in Figure 6.10. After approximately 0.5 h SOC_{OCV} reaches a value of

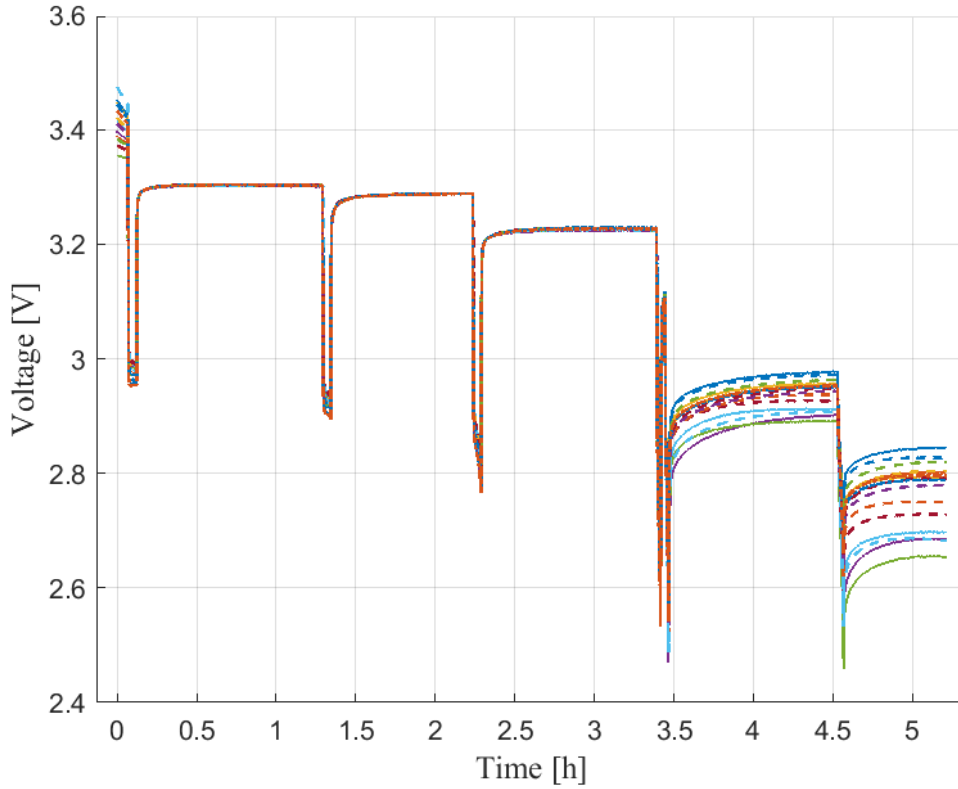


Figure 6.10: $V_{terminal}$ of the 16 LIC:s during the discharge test to evaluate SOC estimation methods.

80 % SOC. Which differs with 7.8 percentage points from $SOC_{ManCalc}$ that reached a value of 72.2 %. The large deviation could partly be a result of inaccuracies in the data used in the look-up table between OCV and SOC. As the voltage drop caused by the impedance in the circuit was estimated, this brings a large uncertainty in how accurate the OCV estimation is. This in combination with the flat voltage curve were a small difference in voltage gives a high impact in SOC estimation, indicates that the OCV method cannot be used during the flat region of the voltage profile. SOC_{OCV} is never stabilised, instead a small decrease in SOC can be seen in the figure. This is a result of not waiting long enough for the voltage to stabilise, but for this application it was determined that the impact would be negligible. Also as the BMS hardware is supplied with power from the batteries, this could also have an impact and decrease the voltage.

The SOC_{CC} and $SOC_{CCEdges}$ are both using the CC method and are discharged to 78.6 %. However this is a deviation of 6.2 percentage points to the $SOC_{ManCalc}$ which dropped to 72.2 %. By debugging the system it was found that the setting of the time period in the QRx was set improperly. The actual time period was measured to be 124 ms and not 100 ms as assumed in the CC algorithms. Using (2.4), with a time period of 124 ms and the current measured by the QRx would give a SOC of 73.7 % which is only 1.5 percentage points from the expected value,

this is therefore responsible for the major part of the error in the SOC estimations using the CC method. The remaining deviation of 1.5 percentage points can partly be explained by the current offset. With $Q_n = 1.076 \text{ Ah}$ and the current offset of 261 mA for 195.3 s , (2.3) gives a drop in SOC with 1.3 percentage units. This indicates that the deviation between the expected value and the CC method is 0.2 percentage units, which is probably a result of measurement errors by the current transducer or inaccuracies in Q_n .

It can be seen that after the discharge, SOC_{CC} and $SOC_{CCEdges}$ are rising, which indicates charging of the LIB. This behaviour is a result of the offset in the current measurement. The next two discharge pulses show similar results as the first one. The current measurement error is accumulated in the current integration, and the OCV method is inaccurate due to the voltage measurement and look-up table data accuracy. These estimation errors, result in a high difference between the three methods.

After the forth discharge, $SOC_{ManCalc}$ gives a SOC of 5 % and $SOC_{CCEdges}$ gives a SOC of 30.7 %, the error is mostly due to the inaccurate time period in the QRx. Once the voltage has stabilised $SOC_{CCEdges}$ is corrected to 3.1 % SOC. Which gives an error of 1.9 percentage units from the expected value. This error is most likely not due to the voltage measurement accuracy or inaccuracy in the look-up table between OCV and SOC since in the low voltage region a large change in voltage is required for a small change in SOC. Instead it is more likely that the large voltage variations between the cells, as can be seen in Figure 6.10, interfere with the estimations. This could result in that the average of Q_n has been miscalculated leading to parameter error in the CC method. As $SOC_{ManCalc} > SOC_{CCEdges}$ this indicates that Q_n has been overestimated which is in line with the analysis in Section 6.1.2.

To study the effect of parameter and measurement errors, simulations were conducted of the system with a load case similar to the discharge test. In Figure 6.12 a constant offset has been applied to the current and each cell voltage measurement of -0.0119 A and 5 mV respectively. The current offset was selected equal to the zero current offset found in the discharge test and the cell voltage offset was selected as an expected measurement error.

The OCV and CC_{Edges} , SOC estimation methods are compared with a ideal SOC calculation using perfect parameters. The figure shows that a small error in the voltage measurement give a large error in the SOC_{OCV} estimation during the flat region of the OCV curve but only a small error at the high and low SOC regions as have previously been suggested. The current offset results in a very small error in the beginning but which stacks over time. This displays the inherent problem with the CC method and the need for frequent calibration.

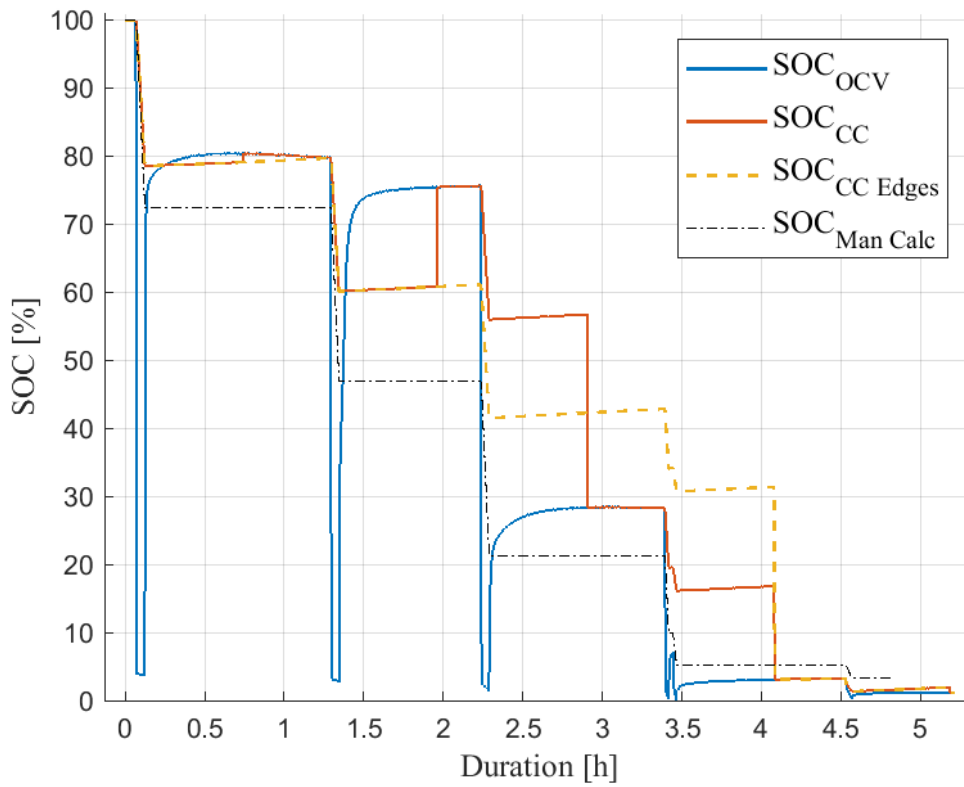


Figure 6.11: SOC estimations using three different methods during the discharge test.

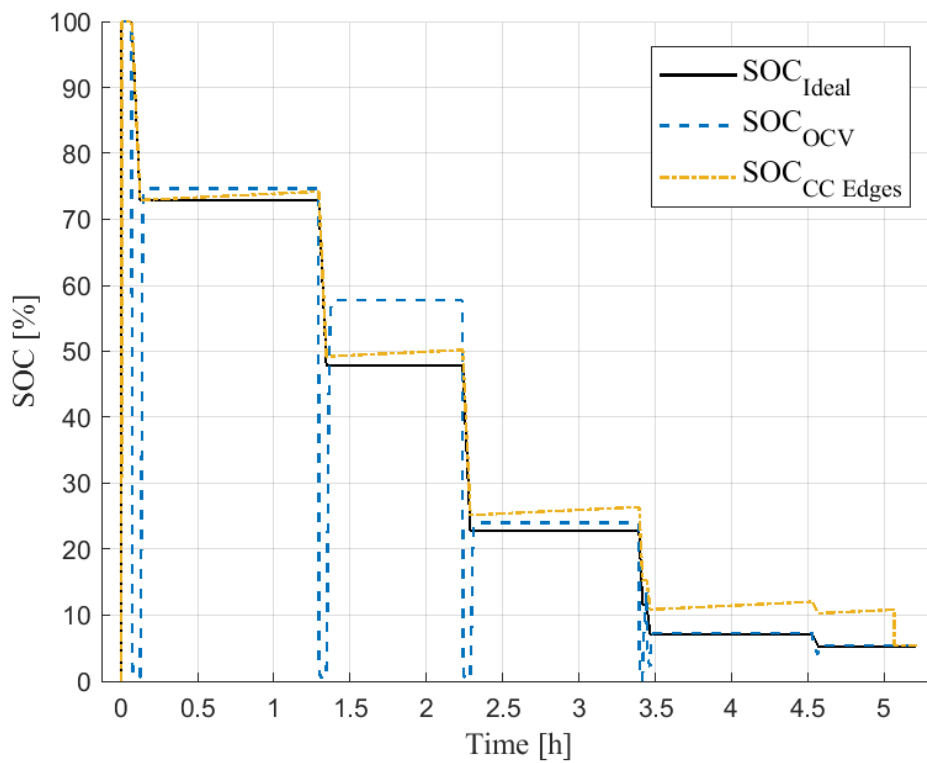


Figure 6.12: Simulation of the BMS with added current and cell voltage offsets of $-0,0119\text{ A}$ and 5 mV respectively. This was run with a similar load case as in the discharge test.

7

Conclusion

Chapter 7 contains the conclusion of this master thesis and recommendations on future work.

7.1 Results from present work

To meet the sustainability goals, the vehicle industry is driven towards EV:s. As EV:s contributes with less greenhouse gases than combustion engines they are preferred. However the production of battery cells contributes with greenhouse gases, pollution of water and mineral resource depletion. With this in mind it is important to reduce the size of the battery as much as possible. To enable this it is important to manage the battery as efficient as possible, to reduce the risk of having to over dimension the battery. Since battery packs are heavy and bulky they are often custom designed for each application. This brings a need for custom designed BMS:s.

The result of this thesis is a custom designed BMS for the go-kart at QRTECH AB. The hardware is scalable as more PCB:s can be inserted in the daisy chain allowing for more LIC:s in multiples of eight to be series connected in the system for a higher or lower system voltage. For the software only minor changes are needed to support for the increased number of cells.

The BMS measures current, voltage and temperature and with this information manages the battery so it stays in the LIC:s narrow operating window. This includes signals for load/charge disconnection to stop the battery from being under-or overcharged. Or disconnection when the temperature and current is to high/low. A passive battery balancer has also been implemented in the BMS.

SOC estimations were done using the OCV method and two versions of the CC method were calibrated by the OCV method. $SOC_{CCEdges}$ were determined to be the most suitable method. This is because it uses the CC method in the flat voltage region of the SOC interval and only calibrates, using the OCV method in the high and low SOC interval, where the voltage change is big for a small change in SOC. The faulty time period of the QRx in combination with the inadequate calibration of the current transducer resulted in low accuracy of the CC model as well. If the time period is set correctly and an algorithm for the current measurement is implemented, the CC method has an acceptable accuracy.

The BMS was tested in a physically and electrically isolated room. Safety precautions were used in the laboratory and the cells were covered with a plexiglas to reduce the risk of short circuit. The LIC:s were monitored so they stayed in the narrow operating window regarding temperature, current and voltage.

7.2 Future work

To increase the accuracy of the CC method, the current transducer should be properly calibrated. An algorithm for the offset should be determined and implemented. The time period on the QRx should also be properly set, preferably dynamical to take into account the difference in computing time between the measurements caused by other processes.

To increase the reliability of the OCV method, a more accurate model of the cell deviation should be evaluated. More LIC:s should be tested to increase the statistical basis to create a more accurate look-up table. To increase the accuracy of the SOC estimation, a more refined method could have been used. For example a Kalman filter as in [5] to account for some of the measurement inaccuracies.

It is also recommended to extract the battery parameters and characteristics using another measuring method. By charging/discharging the battery to a known state and then allowing the battery to reach equilibrium, and repeat the process until the battery is fully charged/discharged. The correlation between SOC and OCV can then be determined. By using this method, the inaccuracies in estimating R_0 and R_1 will not interfere with the accuracy of estimating the OCV curve. It would also be beneficial to extract the battery parameters for different SOC levels as they vary depending on SOC.

As the LIC:s intended for the go-kart did not arrive within the time frame of this thesis, different LIC:s were used to test the BMS. For the BMS to function with the correct cells, the cell characteristics would need to be extracted and incorporated in the software.

SOH estimations were not implemented in this project but would be necessary in the BMS. As the go-kart ages, the capacity of the LIB will decrease and this should be accounted for. The challenges with estimating SOH was determined to be too great to fit the scope of the project.

As the project focused on making a functioning BMS, further work in how to optimise the BMS could be done. For example, could the software be implemented in a more efficient way. As the control system of the BMS was code generated, the optimisation of the software was limited. If the BMS code had been manually written instead, it could most likely have been made more efficient. An example of this is that the voltage over the LIB was calculated three times in the generated code, when in fact it only needs to be calculated once. The SPI communication could have been increased in frequency, resulting in less time for communication but more

losses of data. A weighing on the robustness and the speed of the system should then be made.

The hardware could be made in a more energy efficient way. This project uses a linear regulator to generate 5V for the control circuit which is not the most energy efficient way of regulating the voltage. Also losses in the system could be lowered by optimising the design, using transistors with less losses and so on. A major saving in power could be done by not measuring the voltages and temperatures as often at no load. Since the voltage and temperature measurements are unlikely to change much during no load conditions.

To further improve the simulation set-up, deviations between the LIC:s could be included based on the deviations seen in the measurement data. This could help with determining how to deal with the deviations in the best way.

To further evaluate the system more load cases should be tested at higher loads.

Bibliography

- [1] D. Deng, "Li-ion batteries: basics, progress, and challenges," *Energy Science & Engineering*, vol. 3, (5), pp. 385-418, 2015.
- [2] L. Lu et al, "A review on the key issues for lithium-ion battery management in electric vehicles," *Journal of Power Sources*, vol. 226, pp. 272-288, 2013.
- [3] T. R. Hawkins et al, "Comparative Environmental Life Cycle Assessment of Conventional and Electric Vehicles: LCA of Conventional and Electric Vehicles," *Journal of Industrial Ecology*, vol. 17, (1), pp. 53-64, 2013.
- [4] E. Wikner et al, "Lithium Ion Battery Aging: Battery Lifetime Testing and Physics-Based Modeling for Electric Vehicle Applications." , 2017."
- [5] M. A. Hannan et al, "A review of lithium-ion battery state of charge estimation and management system in electric vehicle applications: Challenges and recommendations," *Renewable and Sustainable Energy Reviews*, vol. 78, pp. 834-854, 2017.
- [6] H. Fisk and J. Leijgård, "A Battery Management Unit," 2010.
- [7] Berg, H. (2015). *Batteries for Electric Vehicles: Materials and Electrochemistry*. Cambridge: Cambridge University Press. doi:10.1017/CBO9781316090978
- [8] K. D. Sadof, L. Mucha and T. C. Frankel, "The hidden costs of cobalt mining," *Washington Post – Blogs*, 2018.
- [9] A. Pehlken, S. Albach and T. Vogt, "Is there a resource constraint related to lithium ion batteries in cars?" *The International Journal of Life Cycle Assessment*, vol. 22, (1), pp. 40-53, 2017.
- [10] H. U. Sverdrup, K. V. Ragnarsdottir and D. Koca, "Integrated Modelling of the Global Cobalt Extraction, Supply, Price and Depletion of Extractable Resources Using the WORLD6 Model," *BioPhysical Economics and Resource Quality*, vol. 2, (1), pp. 1-29, 2017.
- [11] H. U. Sverdrup, "Modelling global extraction, supply, price and depletion of the extractable geological resources with the LITHIUM model," *Resources, Conservation Recycling*, vol. 114, pp. 112-129, 2016.
- [12] B. Swain, "Recovery and recycling of lithium: A review," *Separation and Purification Technology*, vol. 172, pp. 388-403, 2017.
- [13] L. Zhang et al, "Comparative Research on RC Equivalent Circuit Models for Lithium-Ion Batteries of Electric Vehicles," *Applied Sciences*, vol. 7, (10), pp. 1002, 2017.
- [14] L. Lu et al, "A review on the key issues for lithium-ion battery management in electric vehicles," *Journal of Power Sources*, vol. 226, pp. 272-288, 2013.
- [15] W. Chang, "The State of Charge Estimating Methods for Battery: A Review," *ISRN Applied Mathematics*, vol. 2013, pp. 1-7, 2013.

- [16] M. Daowd et al, "Passive and active battery balancing comparison based on MATLAB simulation," in 2011, . DOI: 10.1109/VPPC.2011.6043010.
- [17] LTC6811-1/LTC6811-2 : Multicell Battery Monitors, USA: Linear Technology Corporation, 2016. [Online]. Available: www.linear.com/LTC6811-1, Retrieved: 2018-05-30.
- [18] LTC6820: isoSPI Isolated Communications Interface, USA: Linear Technology Corporation, 2012. [Online]. Available: www.linear.com/LTC6820, Retrieved: 2018-05-30.
- [19] LEM: Automotive current transducer open loop technology DHAB S/118, LEM, 2016. [Online]. Available: www.lem.com/en/dhab-s118, Retrieved: 2018-05-30.
- [20] NTC Thermistors, Murata, 2016. [Online]. Available: www.murata.com, Retrieved: 2018-05-30.

A

Appendix: Figures of the simulation set-up

Figure A.1 shows the total system simulated in Simulink. It shows how the BMS, battery, measuring system, equalising circuit and load models are connected.

Figure A.2 shows how the BMS was modelled in the thesis. With $V_{terminal}$, I , T and Enable Equalising as inputs, $V_{terminal}$, I , T , SOC, Gate control signals, and over/under detection of voltage, temperature and current were set as outputs.

Figure A.3 shows how SOC was modelled in this thesis. With I , $V_{terminal}$ and $T_{average}$ as inputs SOC_{OCV} , SOC_{CC} and $SOC_{CCedges}$ are determined. In the blue box indicated with the name voltage model, one can see the two look-up tables used for determining SOC during charge and discharge respectively. As the battery has to be charged/discharged for a while until the OCV curve of the battery reacts, an integrator is used to determine which look-up table to use.

The battery balancing control model is shown in A.4.

The temperature control model can be seen in Figure A.5. It includes both the conversion from a voltage measurement to temperature as well as over/under temperature detection. The block "Conversion Voltage to resistance" is based on (4.1) and the block "Conversion resistance to temp" is based on (4.2). The over/under detection are the same for temperature, voltage and current and can be seen in Figure A.6.

Figure A.7 shows the battery model. It can be seen that a look-up table determines the OCV depending on SOC and T .

$V_{terminal}$ and I are discretized to simulate measurement every 100 ms as can be seen in Figure A.8.

The battery balancing circuit can be seen in Figure A.9. Depending on the gate signal, the circuit is activated or not.

Figure A.10 shows the load set-up. Different step responses were used to simulate different discharge pulses.

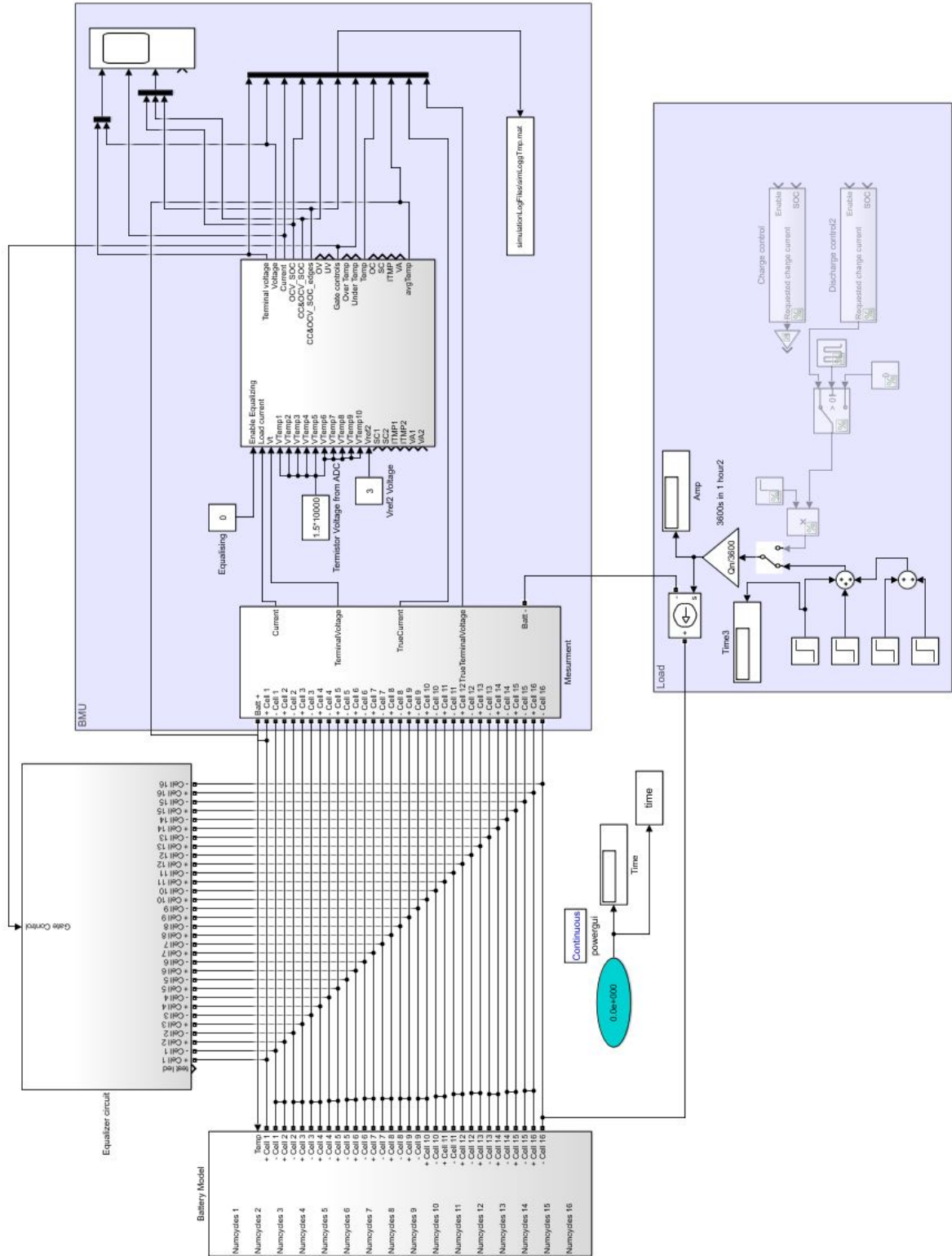


Figure A.1: Total simulation set-up. Including models of the BMS, battery, measuring system, equalising circuit and load.

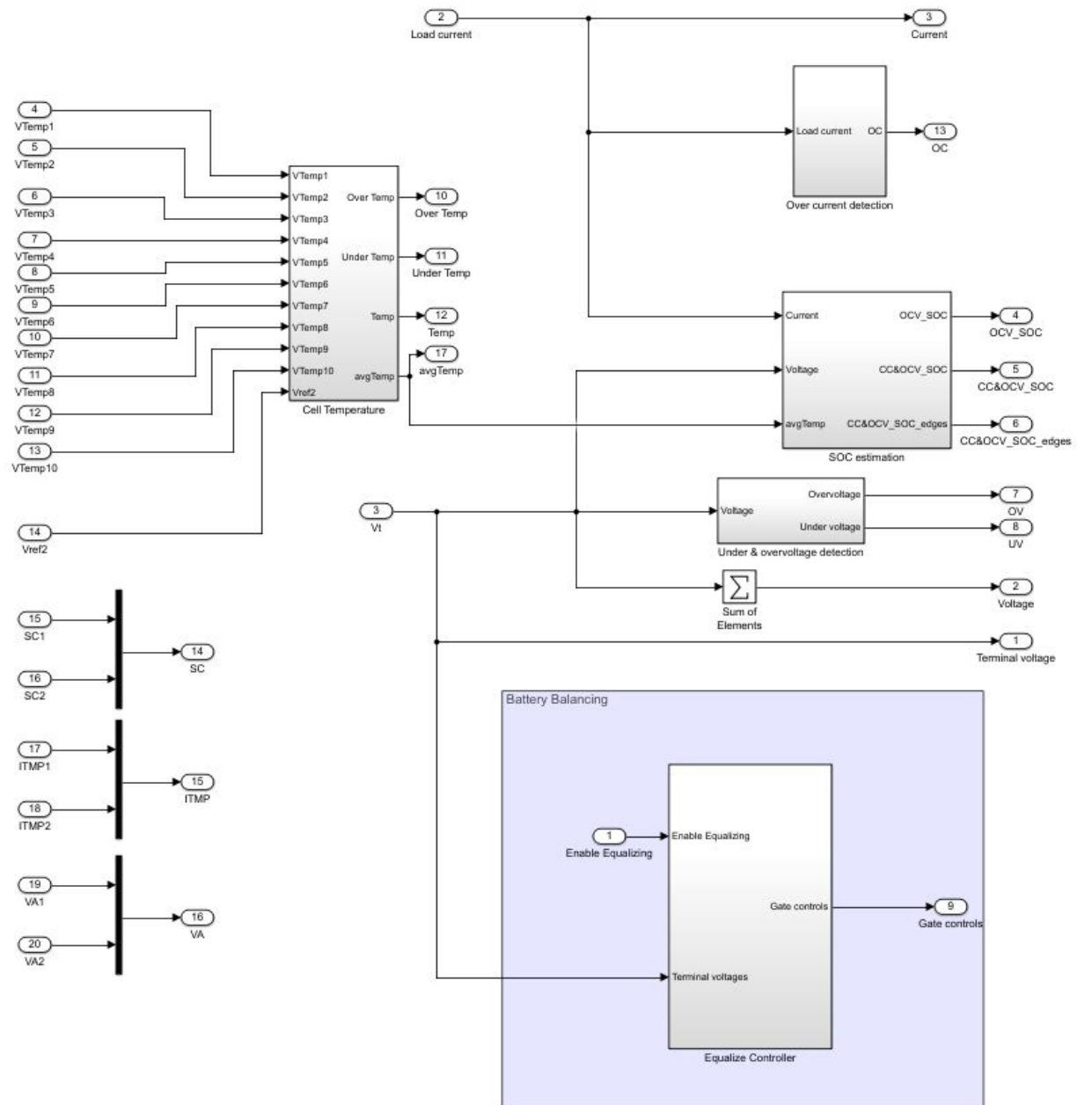


Figure A.2: Overview of the BMS model.

A. Appendix: Figures of the simulation set-up

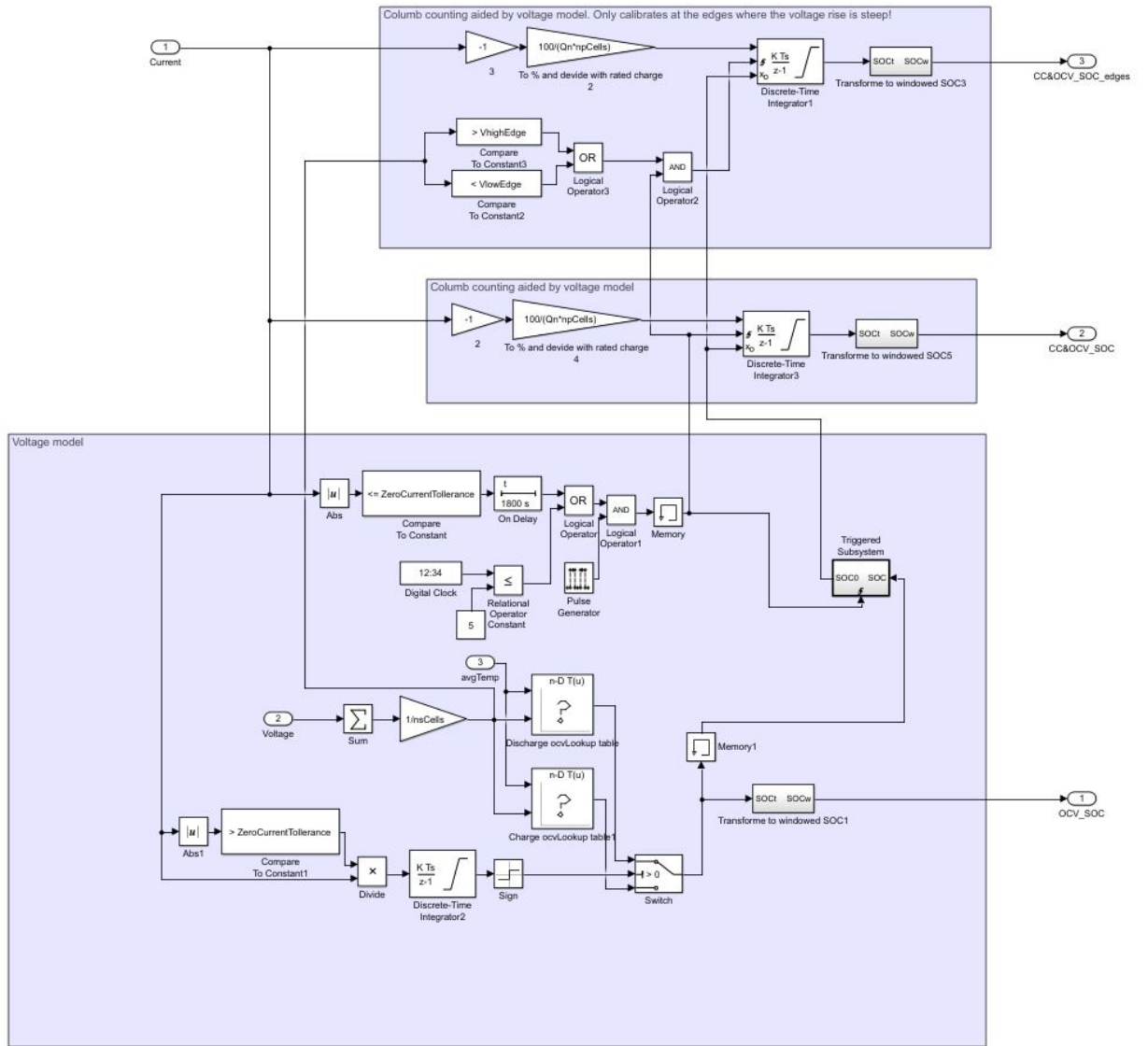


Figure A.3: The SOC estimation model. With I , $V_{terminal}$ and $T_{average}$ as inputs SOC_{OCV} , SOC_{CC} and $SOC_{CCedges}$ are determined.

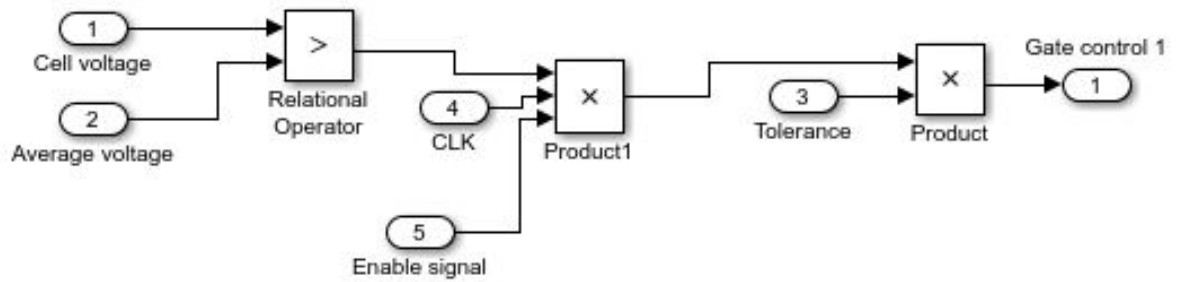


Figure A.4: Battery balancing control model. The gate signal is sent to the battery balancing circuit.

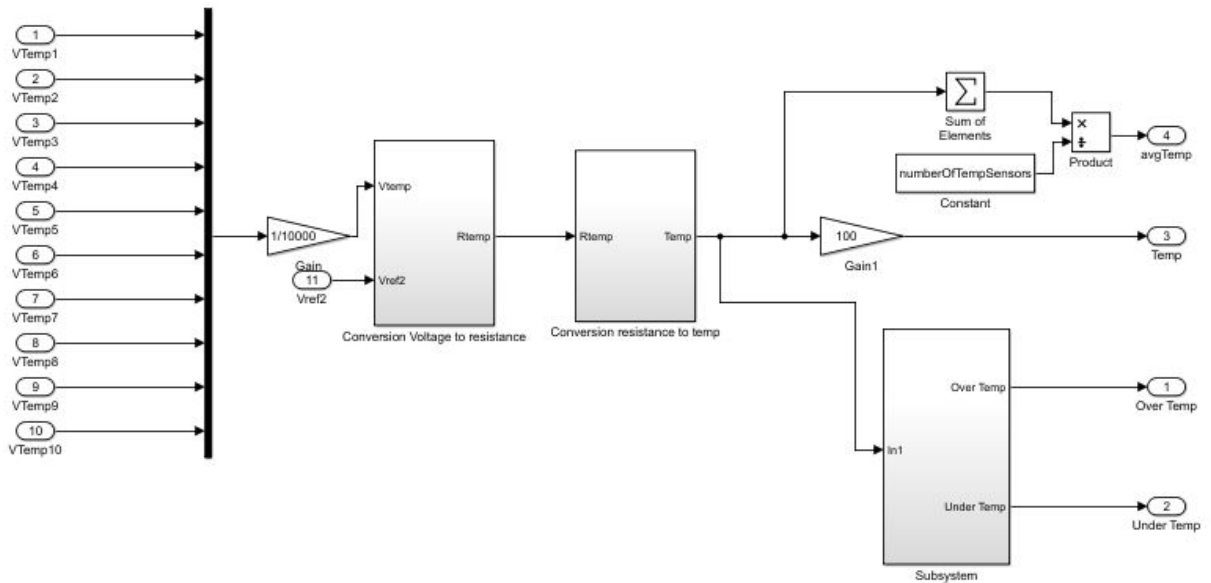


Figure A.5: Temperature control model. Includes both the conversion from a voltage measurement to temperature as well as over/under temperature detection.

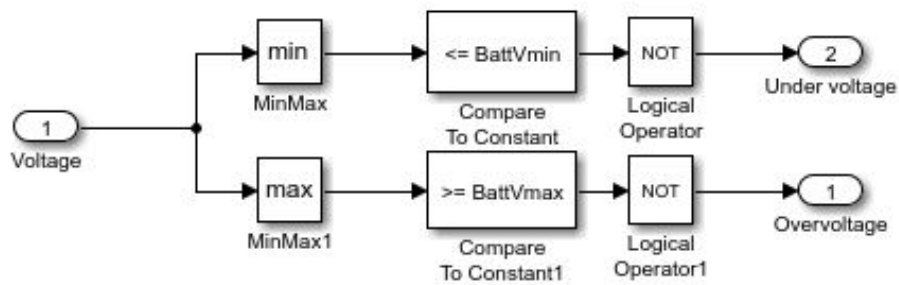


Figure A.6: Over/under voltage detection. The same set-up is used for temperature and current detection as well.

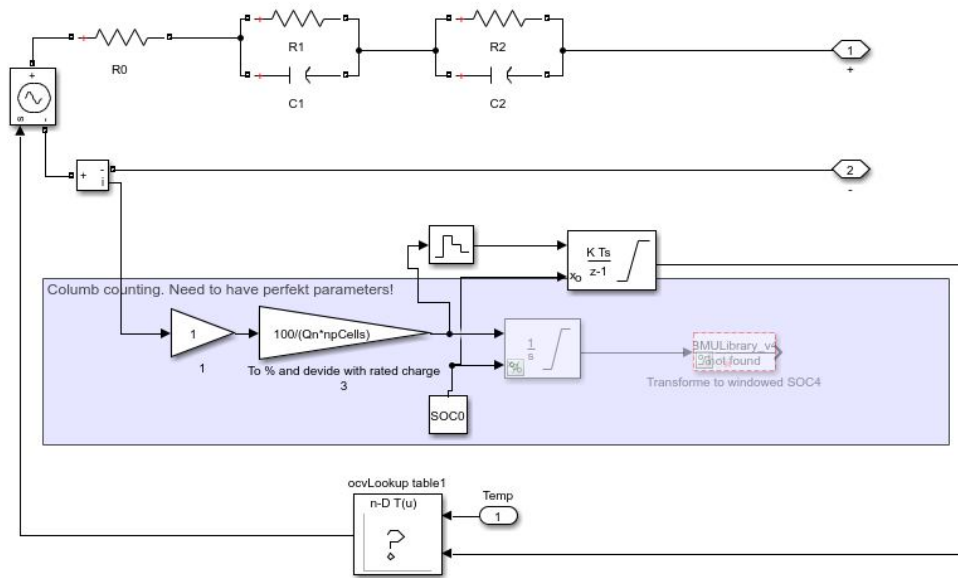


Figure A.7: LIC model.

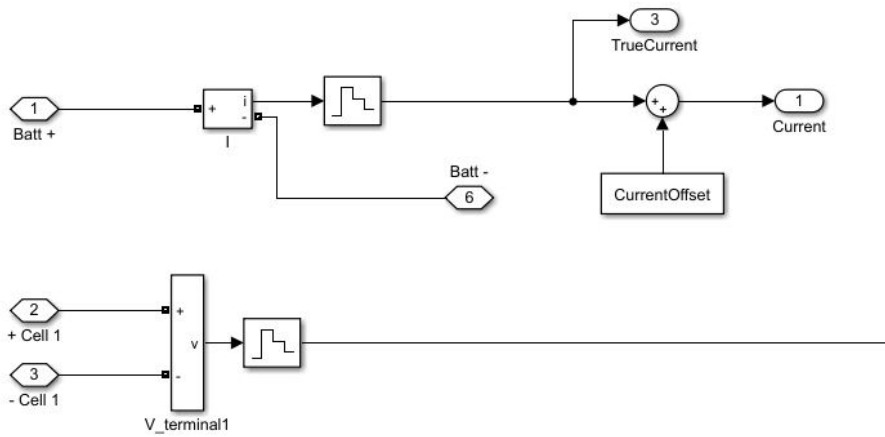


Figure A.8: Discretization of $V_{terminal}$ and I so simulate measurements taken every 100 ms .

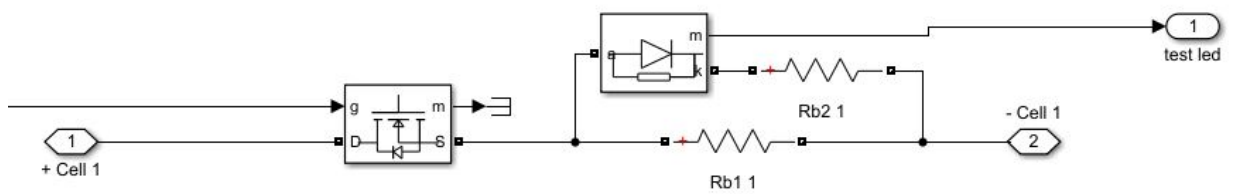


Figure A.9: Battery Balancing circuit

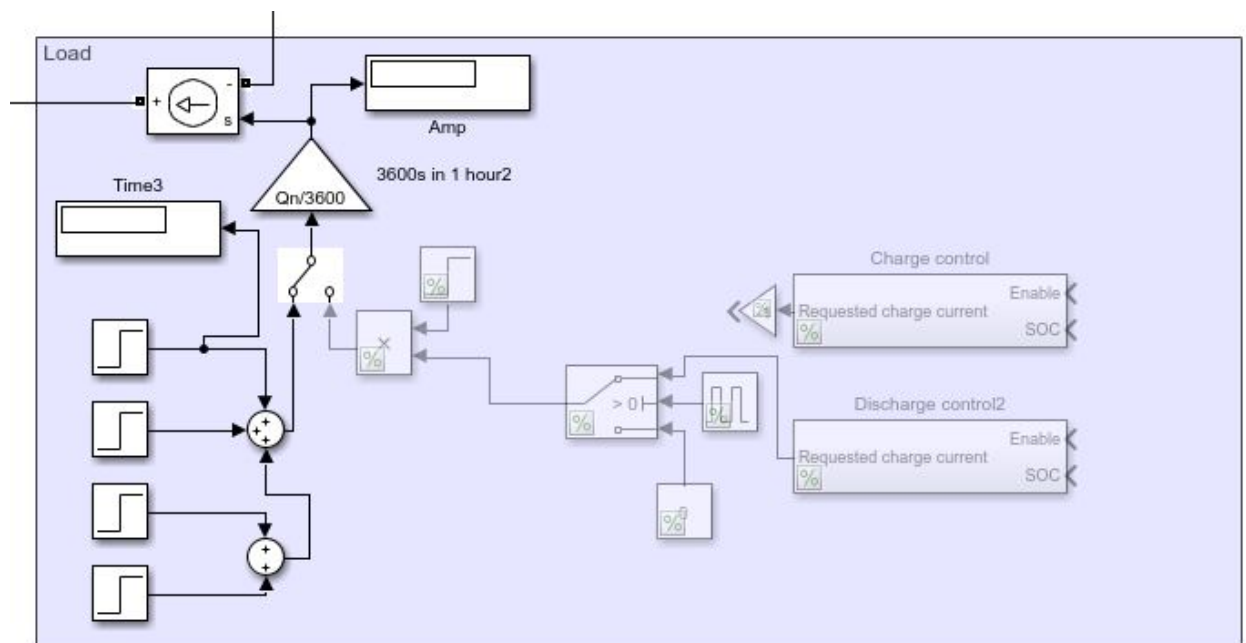


Figure A.10: Load model

B

Appendix: Figures with outliers

Figures with data from or dependant on the data from the LTC6811 suffers from around 4.3 lost measurements per 1 million measurements. This is neglected and filtered out in the report but can be seen here.

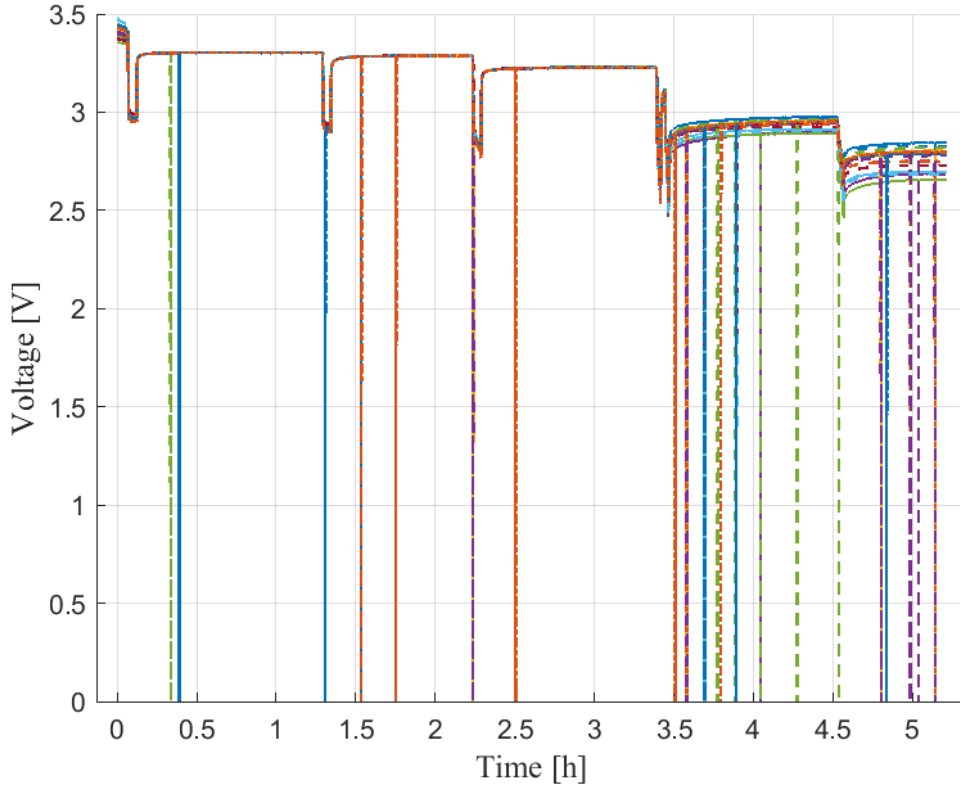


Figure B.1: $V_{terminal}$ of the 16 LIC:s during the discharge test to evaluate SOC estimation methods including outliers.

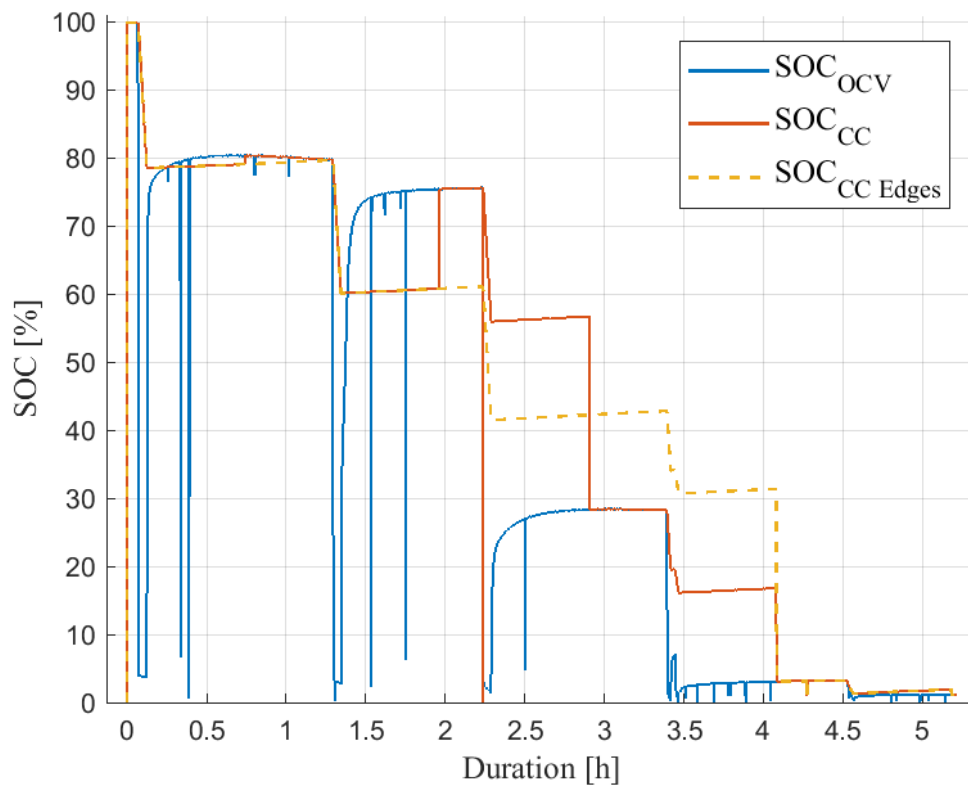


Figure B.2: SOC estimations using three different methods during the discharge test including outliers.

C

Appendix: Datasheet of Headway 40152S cells



HW-40152S 15Ah

Technical Specification

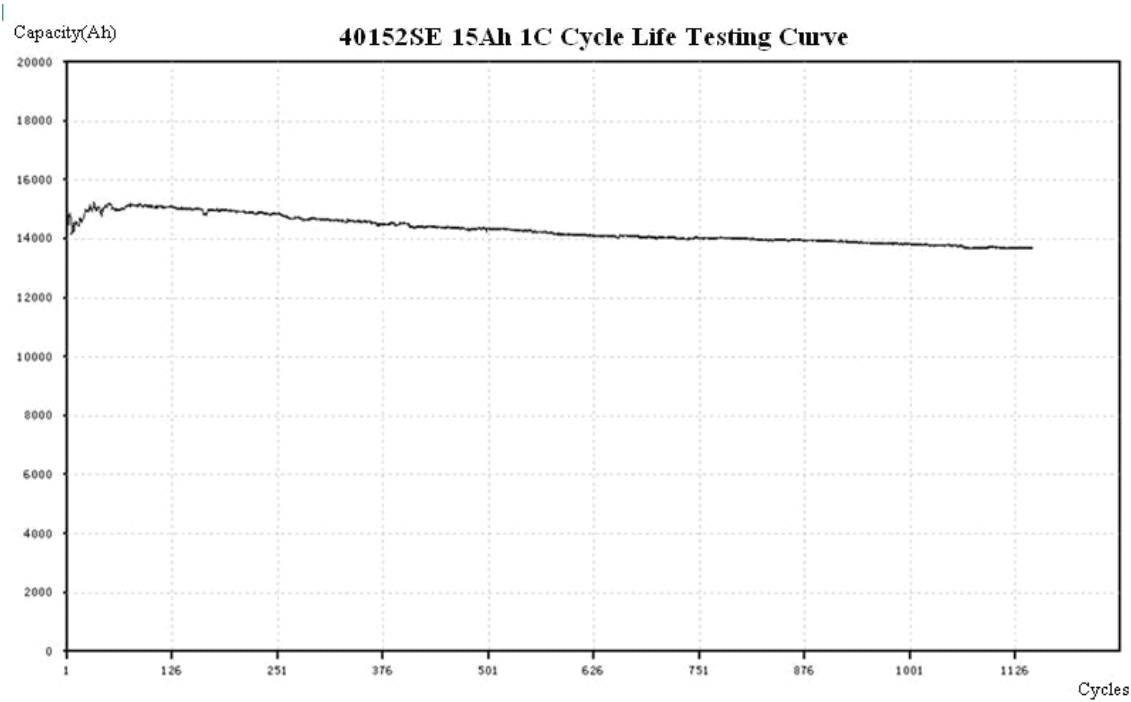
Lithium battery solutions

Specification	
Nominal Voltage	3.2V
Nominal Capacity(0.5C,25°C)	15000mAh
Weight(Approximate)	Approx. 480g
Dimension(Length*Width*Height)	Φ40±1mm*H165±1mm
Standard Discharge	
Max. Continuous Current	5C(75A)
Max. 10 sec. Pulse	10C(150A)
Cut-off Voltage	2.0V
Standard Charge	
Charge Voltage	3.65V±0.05V
Recommended Charge Current	2A
Charge Time	8 hours
Resistance and rates	
Internal Resistance	≤4mΩ
Self-discharge rate	≤5% per Month

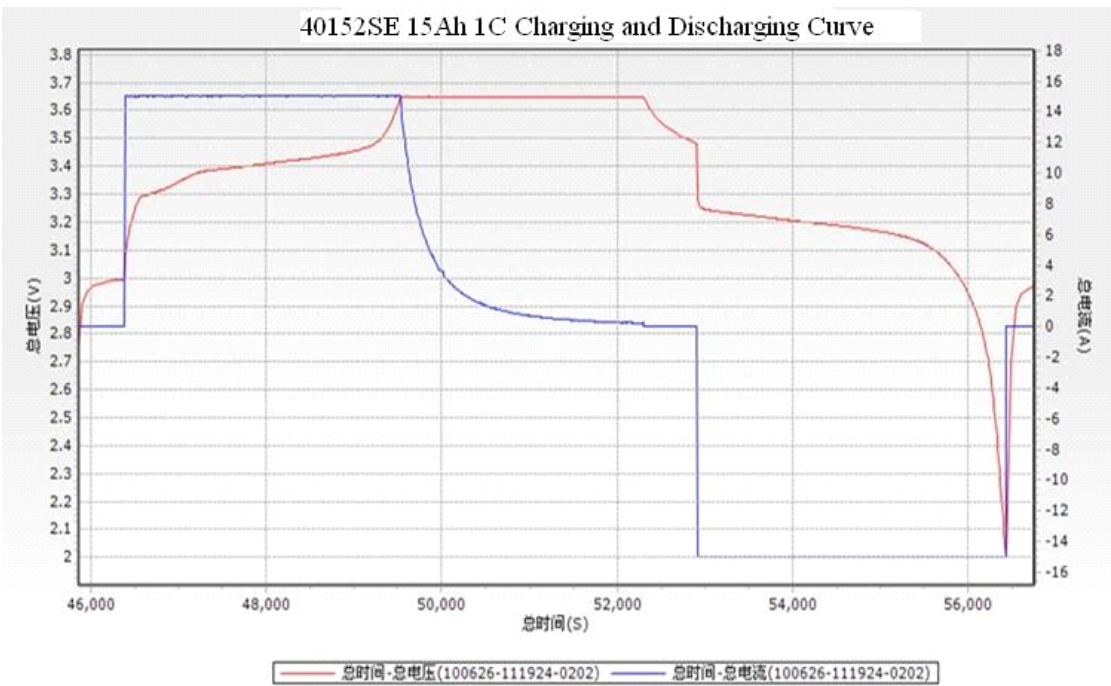


Check with the real products, the specifications are for reference only. It can be designed according to customer's requirements if necessary.

The cycle life testing curve

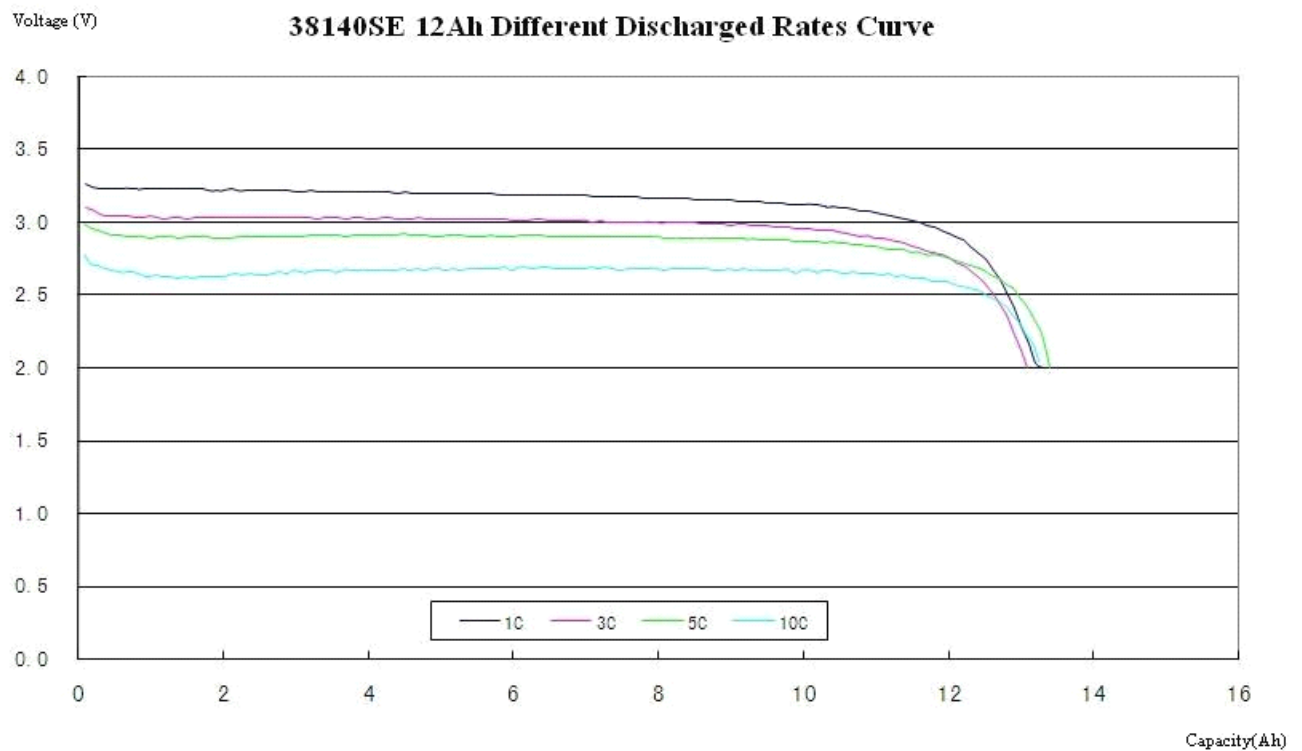


The discharging and charging curve at 1C

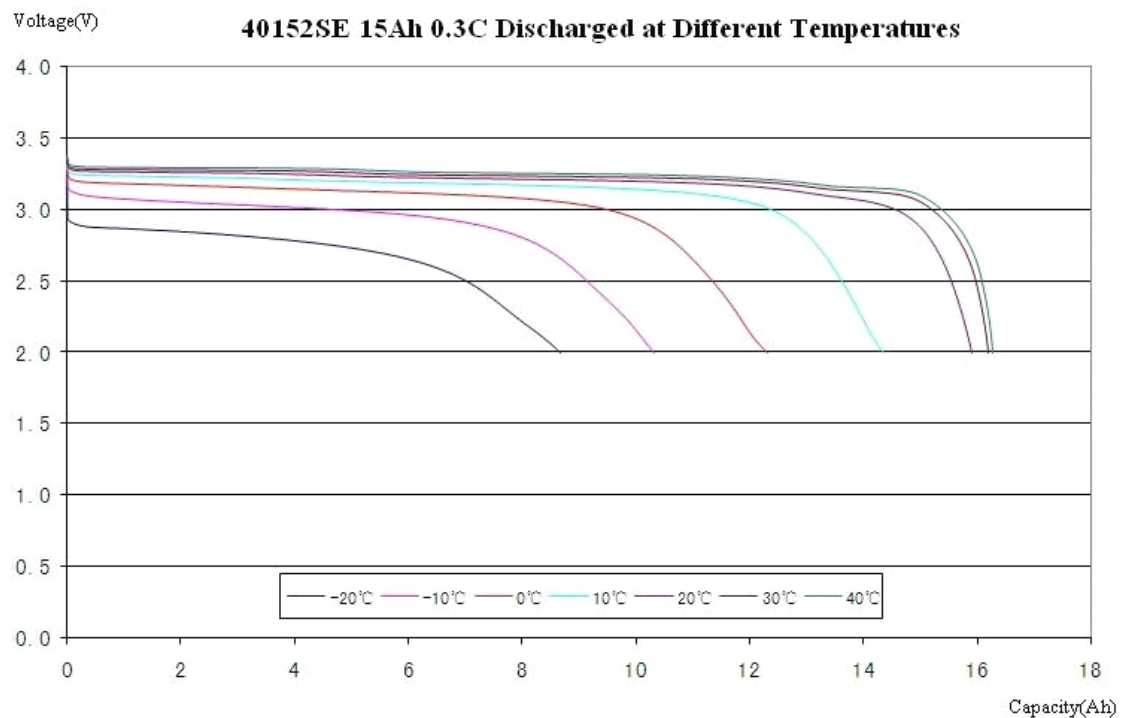


Check with the real products, the specifications are for reference only. It can be designed according to customer's requirements if necessary.

The Different Discharged Rates Curve



0.3C discharged at different temperatures curve



Check with the real products, the specifications are for reference only. It can be designed according to customer's requirements if necessary.

D

Appendix: Datasheet of A123: HTPFR18650-1100mAh-3.2V cells

Product Specification

Product Name: Lithium-ion battery

Model: HTPFR18650-1100mAh-3.2V

Make By: MeiQinghu

Checked By: Zhou Hui

Approved By: Li Tao

Shandong Goldencell Electronics Technology Co., Ltd

Headquarter

Add: Thailand Industrial Park, Hi-tech District, Zaozhuang
City, Shandong Province, China.

Toll-free telephone: 400-812-5699

Tel: +86-632-5296888

Fax: +86-632-5292918

Postcode: 277800

E-MAIL: Market@heter.biz

Branch office (Shenzhen)

Add: 603,6/F., PolyU Base Bldg., Yuexing Road,
Hi-tech Industrial Park, Nanshan, Shenzhen, China

Tel: +86-755-28891995

Fax: +86-755-28892486

Web site: www.heter.biz

Contents

1. Application Scope.....	3
2. Model.....	3
3. Appearance and Dimension.....	3
4. Major Technical Parameters.....	3
5. Characteristics Curves.....	4
6. Safety Characteristics.....	5
7. Environmental Adaptability.....	6
8. Standard Test Environment.....	6
9. Storage and Others.....	7
10. Notice in Using Battery.....	7
Appendix A.....	7

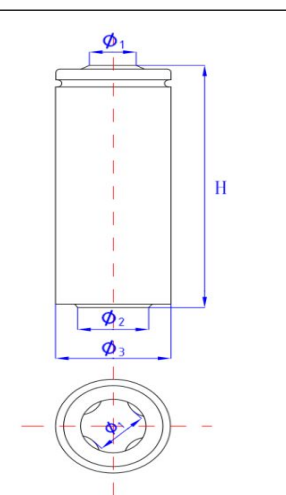
1. Application Scope

This product specification describes product performance indicators of Lithium-ion battery produced by Shandong Goldencell Electronics Technology Co.,Ltd

2. Model

HTPFR18650-1100mAh-3.2V

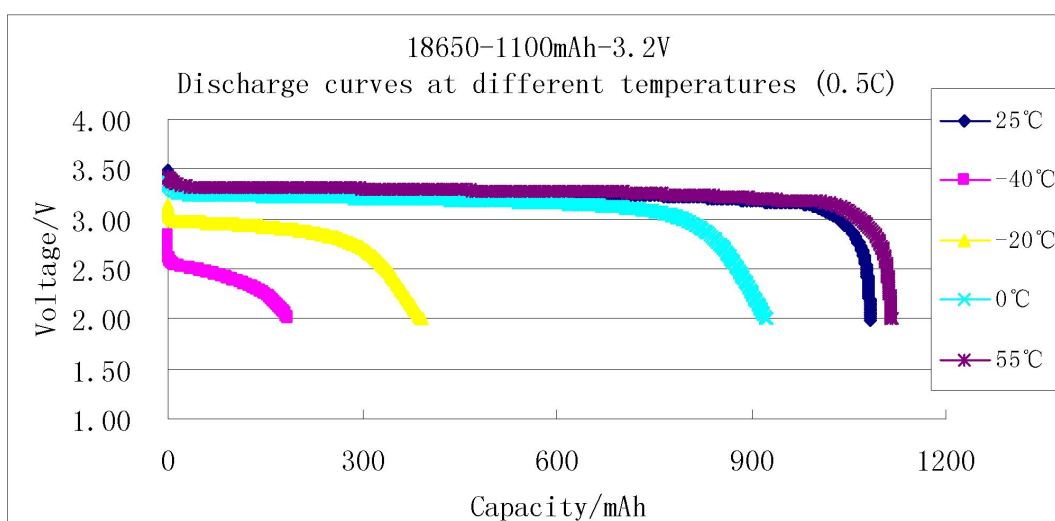
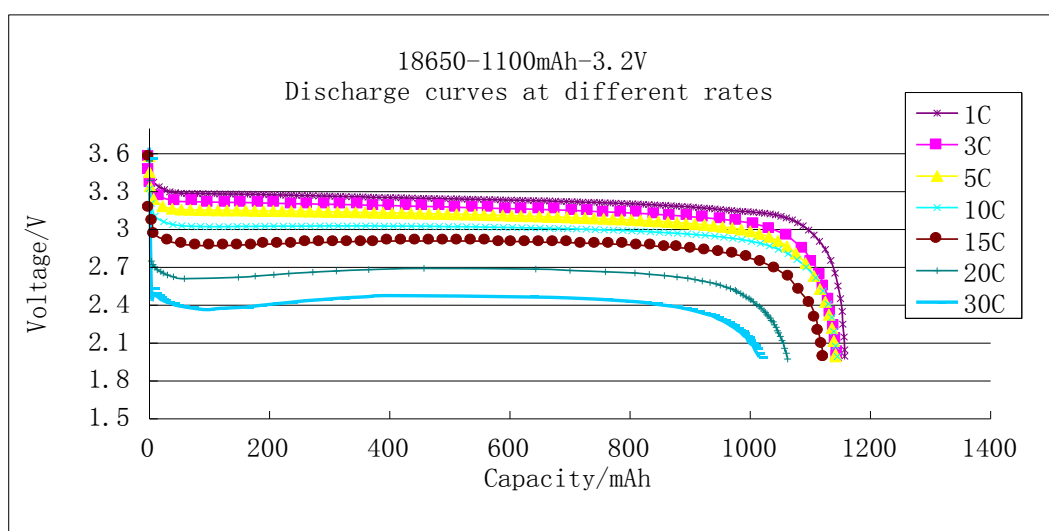
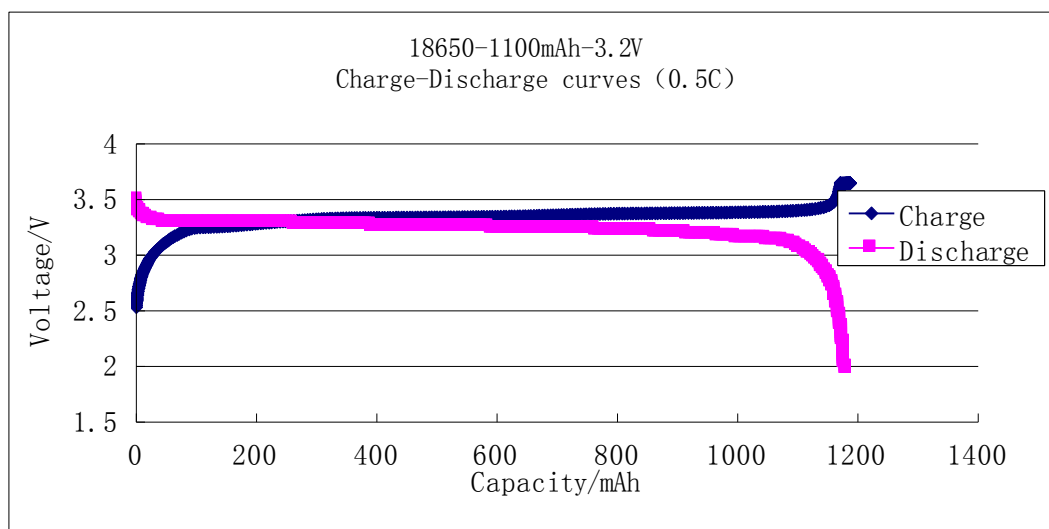
3. Appearance and Dimension

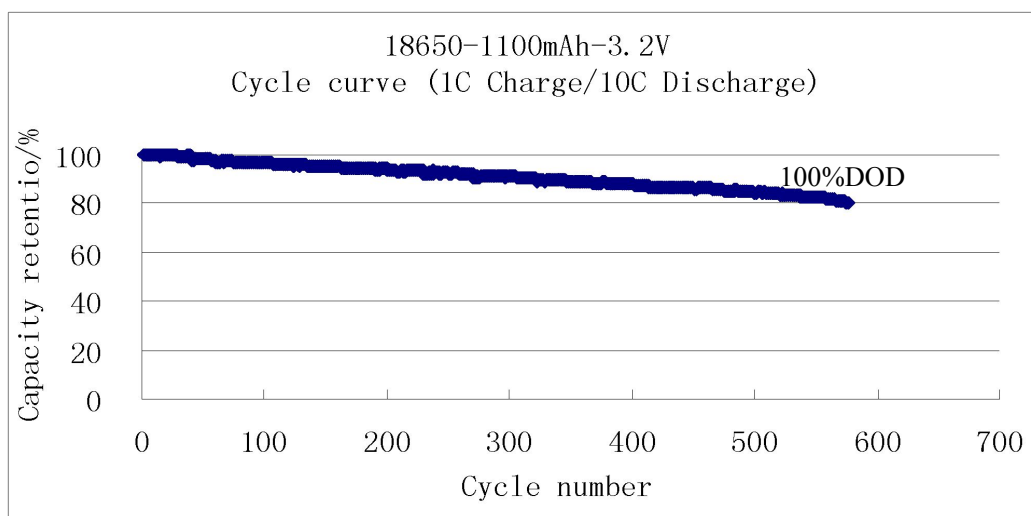
Item	Dimension (mm)	
H	65.2±0.3	
Φ1	8.85 ± 0.15	
Φ2	10 ± 0.2	
Φ3	18.2±0.1	
Sleeving	PET or kraft paper	

4. Major Technical Parameters

No.	Item		Standard	Note
1	Standard Capacity		1100mAh	0.5C,(current value of 1100mA at 1C)
2	Capacity Range		1050~1200mAh	0.5C
3	Standard Voltage		3.2 V	
4	Alternating Internal Resistance		≤18mΩ	
5	Charge Conditions	Cut-off Voltage	3.65±0.05V	constant-current charge to 3.65V at 0.5C, constant voltage charge to stop until 0.01C mA
		Cut-off Current	0.01C	
6	Discharge Cut-off Voltage		2.0V	
7	Cycle Characteristic		500times (100%DOD)	the residual capacity is no less than 70% of rated capacity at 1C Charge , 10C Discharge rate.
			1000 times (80%DOD)	
			3000 times (50%DOD)	
8	Max. charging current		5.5A	
9	Max. Continuous Discharge Current		33A	
10	Pulse Discharge Current		40A, 10s	
11	Working Temperature		Charge:0°C~55°C Discharge:-20°C~60°C	
12	Storage Temperature		-20°C ~ 45°C	Short-term storage (< 3 months)
13	Battery Weight		41 g (Approx.)	

5. Characteristics Curves





6. Safety Characteristics

NO.	Item	Test Method	Standard
1	Overcharge	After normal charge, test the batteries' initial state and capacity. Charge to 10.0V at 3C, then charge at CV mode to 0.01C. Observe battery's variation of appearance.	No explosion, No fire.
2	Over Discharge	After normal charge, test the batteries' initial state. When the batteries are normal, Discharge to 0V at 0.5C. Observe battery's variation of appearance.	No explosion, No fire.
3	External Short-circuit	After normal charge, test the batteries initial state, Keep the battery into explosion protection cover, short-circuit the positive and negative terminals directly (general resistance shall be less than or equal to 50mΩ). Stop the test when the temperature falls to 10℃ lower than the peak value. Observe the variation of the batteries' appearance and temperature.	No explosion, No fire.
4	Thermal Abuse	Test the batteries' initial state and capacity. Standard charge. Put battery into oven, increase the temperature to 130±2℃ at rate of (5±2℃) /min, and keep it for 30min. Observe the variation of batteries' appearance.	No explosion, No fire.
5	Drop	After normal charge, test the batteries' initial state and capacity. Then let it fall from a height of 1m (the lowest height) to a smooth cement floor, twice.	No explosion, No fire.
6	Heavy Impact	A diameter of 15.8 mm steel rod is placed in the middle of the fully charged battery, then the weight of 10Kg hammer from 1.0m height free falls to the battery upper.	No explosion, No fire.
7	Extrusion Test	Place the battery in between the pressing surface of extrusion apparatus, parallel the axes of cylindrical battery to the pressing surface, and gradually increase pressure up to 13KN, keeping the pressure for 1min.	No explosion, No fire.

8	Prick test	Use $\Phi 3$ mm to 5 mm high temperature resistant steel needle, to 10 mm/s ~ 40 mm/s of speed, from the perpendicular to the direction of the battery plate(Steel needle stops in the battery).	No explosion, No fire.
---	------------	--	---------------------------

7. Environmental Adaptability

NO.	Item	Test Method	Standard
1	Temperature Cycle	Store the battery for 48 hours at $75\pm 2^{\circ}\text{C}$ after standard charge, then store the battery at -20°C for 6 hours, and at room temperature for 24 hours. Observe the batteries' appearance.	No leakage, No smoke, No fire, No explosion.
2	Static Humidity	Put the battery at $40^{\circ}\text{C}\pm 5^{\circ}\text{C}$ and 95%RH chamber for 48h, then get it out and store it for 2h at room temperature. Observe the appearance and discharge at 0.5C to 2.0V, then test the final capacity.	Discharge capacity after storage is more than 90% of rated capacity. No obvious outside damage, No corrosion, No smoke, No explosion
3	Vibration	Standard charge. Equip it to the vibration platform, prepare the test equipment according to following vibration frequency and relevant swing, doing frequency sweeping from X, Y, Z three directions, each from 10Hz to 55Hz for 30 minutes of recycling, rating of which is 1oct/min: A)vibration frequency:10Hz~30Hz Displacement breadth (single swing): 0.38mm B)vibration frequency:30Hz~55Hz Displacement breadth (single swing): 0.19mm. Observe the final state after scanning.	Residual Capacity $\geq 90\%$ Rated Capacity Voltage Decrease Rate $\leq 0.5\%$ No obvious outside damage, No leakage, No smoke, No explosion.
4	Normal Storage	Test the batteries' initial state and capacity; store the battery for 30 days after standard charge, test the final state. Discharge at 0.5C to 2.0V, then test batteries' residual capacity. Then after normal charge, discharge at 0.5C to 2.0V, then test the batteries' recovery capacity, Three cycles are permitted for this test, If one of the three cycles can reach the standard, it represents the battery has reached the standard.	Residual Capacity $\geq 90\%$ Initial Capacity Recuperative Capacity $\geq 95\%$ Initial Internal

8. Standard Test Environment

Unless especially specified, all tests stated in this Product Specification are conducted at below condition:

Temperature: $25\pm 2^{\circ}\text{C}$

Humidity: $(65\pm 20)\%$ RH

9. Storage and Others

9.1 Long Time Storage

If the battery is stored for a long time (more than three months), the battery should be stored in dry and cool place. The battery should be charged and discharged every three months. The batteries' storage voltage should be 3.3~3.4V and the battery should be stored in a condition as NO.8.

9.2 Others

Any matters that this specification does not cover should be consulted between the customer and Goldencell.

10. Notice in Using Battery

Please pay attention to followings in case of battery will have leakage, heat etc.

- Do not immerse the battery in water or seawater, and keep the battery in a cool dry surrounding if it stands by.
- Do not use or leave the battery at high temperature as fire or heater. Otherwise, it can overheat or fire or its performance will be degenerate and its service life will be decreased.
- Do not reverse the position and negative terminals.
- Do not connect the battery electrodes to an electrical outlet.
- Do not short circuit. Otherwise it will cause serious damage of the battery.
- Do not transport or store the battery together with metal objects such as hairpins, necklaces, etc.
- Do not strike, trample, throw, fall and shock the battery.
- Do not directly solder the battery and pierce the battery with a nail or other sharp objects.
- Do not use the battery in a location where static electricity and magnetic field is great, otherwise, the safety devices may be damaged, causing hidden trouble of safety.
- Use the battery charger specifically when recharging.
- If the battery leaks and the electrolyte gets into the eyes, do not rub the eyes, instead, rinse the eyes with clean water, and immediately seek medical attention. Otherwise, it may injure eyes.
- If the battery gives off strange odor, generates heat, becomes discolored or deformed, or in any way appears abnormal during use, recharging or storage, immediately stop charging, using, and remove it from the device.
- In case the battery terminals are dirty, clean the terminals with a dry cloth before use. Otherwise poor performance may occur due to the poor connection with the instrument.
- Tape the discarded battery terminals to insulate them.

Note

The following is the interpretation of some terms in the above test project:

- (1) Standard charge: Under the environment of $25^{\circ}\text{C}\pm 2^{\circ}\text{C}$, for constant current battery charging 0.5 C to cut-off voltage, to a constant voltage charging to the cut-off current, stop charging.
- (2) Initial state: Initial state of voltage and internal resistance of the battery.
- (3) Final state: State of battery internal resistance and voltage.
- (4) Residual Capacity: The first discharge capacity batteries after a specific test.
- (5) Recovery Capacity: The discharge capacity by specifically charge-discharge cycle repeatedly after being tested by the specific procedure.

Appendix A

Suggestions for Battery Packs

1、Selecting principle of nickel strip is often applied to the design of battery packs.

Based on the working current of battery packs to make the shunt selection of nickel strip. The common nickel strip could under the current as below:

Nickel Strip Type	3*0.1	4*0.1	7*0.15	8*0.15
Normal Working Current	2A	3A	7A	8A
Maximum Continues Current	4A	5A	13A	15A

2、Relation between the battery packs design current and lead wires current breakdown, and principle of wires selection.

Based on the working current of battery packs to make the shunt selection of wires. Different wires could under the current as below:

AWG	外径		截面积	电阻值	正常电流	最大电流	AWG	外径		截面积	电阻值	正常电流	最大电流
	公制mm	英制inch	(mm ²)	(Ω/km)	(A)	(A)		公制mm	英制inch	(mm ²)	(Ω/km)	(A)	(A)
0000	11.68	0.46	107.22	0.17	423.2	482.6	22	0.643	0.0253	0.3247	54.3	1.280	1.460
000	10.4	0.4096	85.01	0.21	335.5	382.6	23	0.574	0.0226	0.2588	48.5	1.022	1.165
00	9.27	0.3648	67.43	0.26	266.2	303.5	24	0.511	0.0201	0.2047	89.4	0.808	0.921
0	8.25	0.3249	53.49	0.33	211.1	240.7	25	0.44	0.0179	0.1624	79.6	0.641	0.731
1	7.35	0.2893	42.41	0.42	167.4	190.9	26	0.404	0.0159	0.1281	143	0.506	0.577
2	6.54	0.2576	33.62	0.53	132.7	151.3	27	0.361	0.0142	0.1021	128	0.403	0.460
3	5.83	0.2294	26.67	0.66	105.2	120.0	28	0.32	0.0126	0.0804	227	0.318	0.362
4	5.19	0.2043	21.15	0.84	83.5	95.2	29	0.287	0.0113	0.0647	289	0.255	0.291
5	4.62	0.1819	16.77	1.06	66.2	75.5	30	0.254	0.01	0.0507	361	0.200	0.228
6	4.11	0.162	13.3	1.33	52.5	59.9	31	0.226	0.0089	0.0401	321	0.158	0.181
7	3.67	0.1443	10.55	1.68	41.6	47.5	32	0.203	0.008	0.0316	583	0.128	0.146
8	3.26	0.1285	8.37	2.11	33.0	37.7	33	0.18	0.0071	0.0255	944	0.101	0.115
9	2.91	0.1144	6.63	2.67	26.2	29.8	34	0.16	0.0063	0.0201	956	0.079	0.091
10	2.59	0.1019	5.26	3.36	20.8	23.7	35	0.142	0.0056	0.0169	1200	0.063	0.072
11	2.3	0.0907	4.17	4.24	16.5	18.8	36	0.127	0.005	0.0127	1530	0.050	0.057
12	2.05	0.0808	3.332	5.31	13.1	14.9	37	0.114	0.0045	0.0098	1377	0.041	0.046
13	1.82	0.072	2.627	6.69	10.4	11.8	38	0.102	0.004	0.0081	2400	0.032	0.036
14	1.63	0.0641	2.075	8.45	8.2	9.4	39	0.089	0.0035	0.0062	2100	0.025	0.028
15	1.45	0.0571	1.646	10.6	6.5	7.4	40	0.079	0.0031	0.0049	4080	0.019	0.022
16	1.29	0.0508	1.318	13.5	5.2	5.9	41	0.071	0.0028	0.004	3685	0.016	0.018
17	1.15	0.0453	1.026	16.3	4.1	4.7	42	0.064	0.0025	0.0032	6300	0.013	0.014
18	1.02	0.0403	0.8107	21.4	3.2	3.7	43	0.056	0.0022	0.0025	5544	0.010	0.011
19	0.912	0.0359	0.5667	26.9	2.6	2.9	44	0.051	0.002	0.002	10200	0.008	0.009
20	0.813	0.032	0.5189	33.9	2.0	2.3	45	0.046	0.0018	0.0016	9180	0.006	0.007
21	0.724	0.0285	0.4116	42.7	1.6	1.9	46	0.041	0.0016	0.0013	16300	0.005	0.006

3、Voltage protection point value (for single cell) of protection board or BMS, and selecting principle of protection board.

	Over-charged Protection Voltage	Over-discharged Protection Voltage	The protection voltage point for monomer should be selected also based on the safety voltage point of cell and protection voltage point of IC.
Lithium Iron Phosphate	3.6-3.9	2.0-2.5	
Ni-Co- Mn	4.05-4.25	2.5-3.0	
Selecting principles of protection board: based on the safety needs of the cell and customers' requirements. To select the suitable protection board according to the size of battery packs.			

4、Selecting principles of chargers

Selecting principles of chargers

- (1) Voltage should be regulated by the safest voltage of chargeable cell * n (make the Lithium iron phosphate as 3.6 V and Ni- Co- Mn as 4.2 V);
- (2) Current should be limited by the safe current of chargeable cell, and the customers' specific requirements also should be considered.
- (3) If above 120W, chargers with aluminium alloy cooling fin or cooling fan will be suggested.
- (4) If under 60W, chargers with plastic shell will be suggested.

5、In the process of packs structure design and production, some measures and skills could be handled to avoid battery short circuit.

- (1) To strengthen the positive insulation treatment of the monomer batteries, with barley paper or other high temperature resistant material;
- (2) Battery in the case of size allowed, should try to use batteries of the isolation.
- (3) Battery when working current is larger and can't use bracket, should strengthen the insulation of the batteries shell, for example, using paper sleeve, PVC casing.
- (4) The power line shall not directly contact with the surface of the batteries, avoid cross; Must cross the line and the line between the bracket with high temperature tape or barley paper.
- (5) Power line is not connected to the nickel spot welding surface as far as possible, cannot be avoided, the power line between nickel and high temperature insulation tape to stick a highland barley paper.
- (6) The reasonable design of nickel welding way, minimize nickel piece of calorific value.